

Searches for Electroweak Production of Compressed
Supersymmetry in Events with Soft Leptons Plus Missing
Transverse Momentum and Hard Jet Recoil

Sheena Calie Schier

Contents

1	Introduction	3
2	The Standard Model of Particle Physics and Additional Theories	4
2.1	Forces and Particles	4
2.2	Mathematical Formalism of the Standard Model	4
2.3	Gauge Symmetries and Spontaneous Symmetry Breaking	4
2.4	Higgs Mechanism and Gauge Boson Masses	4
2.5	Shortcomings of the Standard Model	5
2.5.1	Darkmatter	5
2.6	Supersymmetry	5
2.7	Phenomenology of Direct Production of Higgsinos and Sleptons in Compressed Scenarios	5
3	ATLAS Experiment	6
3.1	Tracking	6
3.1.1	Pixel Detector	6
3.1.2	Semi-Conductor Tracker	6
3.1.3	Transition Radiation Tracker	6
3.2	Calorimetry	6
3.2.1	Electromagnetic Calorimeter	6
3.2.2	Hadronic Calorimeter	6
3.3	Muon System	6
3.4	DAQ and Trigger	6
4	MC and Data samples	7
4.1	Signal Samples	7
4.2	Triggers	10
4.2.1	MET Triggers	10
4.2.2	Combined Triggers	10
5	Event Selection and Signal Regions	12
5.1	Object Definitions	12
5.2	Discriminating Variables	14
5.3	Signal Regions	14
5.3.1	Slepton Signal Regions	14
5.3.2	Higgsino Signal Regions	14

6	Fake Factor Method	18
6.1	Introduction	18
6.2	Fake Factor Method	20
6.3	Fake Factor Method Applied to Low- p_T Di-lepton Events	21
6.3.1	Fake Factor Monte Carlo Studies	21
6.3.2	Electron Fake Factors	31
6.3.3	Muon Fake Factors	37
7	Backgrounds	49
7.1	Fake Lepton Background	49
7.2	$t\bar{t}$ Background	49
7.3	Drell-Yan Background	49
7.4	Z+jets Background	51
8	Systematic Uncertainties	61
8.1	Experimental	61
8.2	Theoretical	61
9	Results	66
9.1	Compressed Higgsino	67
9.2	Compressed Slepton	68
10	Conclusion	70

1 Introduction

Particle accelerators have been around since such and such time and have been the source of the most precise physics measurements and lead to deeper understanding of the most fundamental forces and particles in nature. Discovery of top quarks at this collider and the W and Z bosons. Da da da LEP e^+e^- machine blah blah. The Large Hadron Collider pushing into unseen energy realms has the imminent task of finding the Higgs boson, but that is not all. There must be more, and it was believed for decades new physics was right around the corner from LEP(and others).

2 The Standard Model of Particle Physics and Additional Theories

The universe seems like a very complex place made out of many types of material that interacts by various complex mechanisms. Although this will always remain true, particle physics has constructed a theory that incorporates all fundamental particles and explains their existence and interactions in simplicity through the field equations that describe the fundamental forces in the universe. This theory is called the Standard Model of Particle Physics and, apart from the absence of gravity which is far too weak to be described by particle interactions, is fundamentally complete.

2.1 Forces and Particles

The Standard Model describes three of the four known fundamental forces of our universe; electromagnetic force, the strong force, and the weak force. It leaves out the gravitational force only because the energy scale at which gravity does its business is so many orders of magnitude below the other forces that there are intrinsic incompatibilities in their description of particle interactions. According to experiment, there are only a hand full of fundamental particles, among which can be separated into two distinct categories: fermions and bosons. These two types of particles play completely different roles in the state and phenomena of the universe. [Tul11]

You and I and the entire world we experience is comprised of fermions, spin $\frac{1}{2}$ Dirac particles, that can be further categorized as leptons and quarks depending on their intrinsic propensity to interact with a given fundamental force field or not. The lepton family consists of three types of electron (e, μ, τ) and their associated neutrino partners (ν_e, ν_μ, ν_τ).

2.2 Mathematical Formalism of the Standard Model

Field equations and fermion and boson interactions.

2.3 Gauge Symmetries and Spontaneous Symmetry Breaking

$$U(1)_Y \times SU(2)_L \times SU(3)_S$$

2.4 Higgs Mechanism and Gauge Boson Masses

Explain local $SU(2)$ gauge symmetry breaking, the production of the Higgs boson and how this allows for massive weakly interacting gauge bosons.

2.5 Shortcomings of the Standard Model

2.5.1 Darkmatter

One alarming problem with the Standard Model is its incapability the explain dark matter.

2.6 Supersymmetry

Extension of the Poincare Group which leads to boson-fermion symmetry.

2.7 Phenomenology of Direct Production of Higgsinos and Sleptons in Compressed Scenarios

Here talk about the discriminating variables for the higgsino and slepton signal regions (mll and mt2).

3 ATLAS Experiment

The Large Hadron Collider (LHC) is a 27 km long circular proton accelerator with proton beams moving in opposite directions around the ring at speeds near 99.99% the speed of light. The beams travel around the ring in separate vacuum beam pipes and are accelerated and directed around the ring using gigantic semi-conducting magnets. To reach LHC energies the proton beams are accelerated in smaller accelerator structures gradually increasing in size until they are injected into the LHC, which is still the largest and most powerful accelerator in the world. The beams are made to collide at 4 different interaction points at which there are 4 different detector experiments: ALICE, LHC-B, CMS, and ATLAS.

3.1 Tracking

3.1.1 Pixel Detector

Inner most pixelated tracker.

3.1.2 Semi-Conductor Tracker

Middle silicon strip tracker.

3.1.3 Transition Radiation Tracker

Outer most straw tube tracker.

3.2 Calorimetry

3.2.1 Electromagnetic Calorimeter

Measures energy of electromagnetic objects.

3.2.2 Hadronic Calorimeter

Measures energy of hadronic objects

3.3 Muon System

An outer tracker dedicated entirely to tracking muons.

3.4 DAQ and Trigger

Complex computing system to acquire and store data.

4 MC and Data samples

Can talk about integrated lumi and maybe event weight

The event weights are very important. Currently I am applying the total weight as:

$$totalWeight = ttbarNNLOWeight * pileupWeight * eventWeight * leptonWeight * jvtWeight * bTagWeight \quad (1)$$

The weights are recalculated during the merging phase using the cross-section and the sumOfWeightsHist.

4.1 Signal Samples

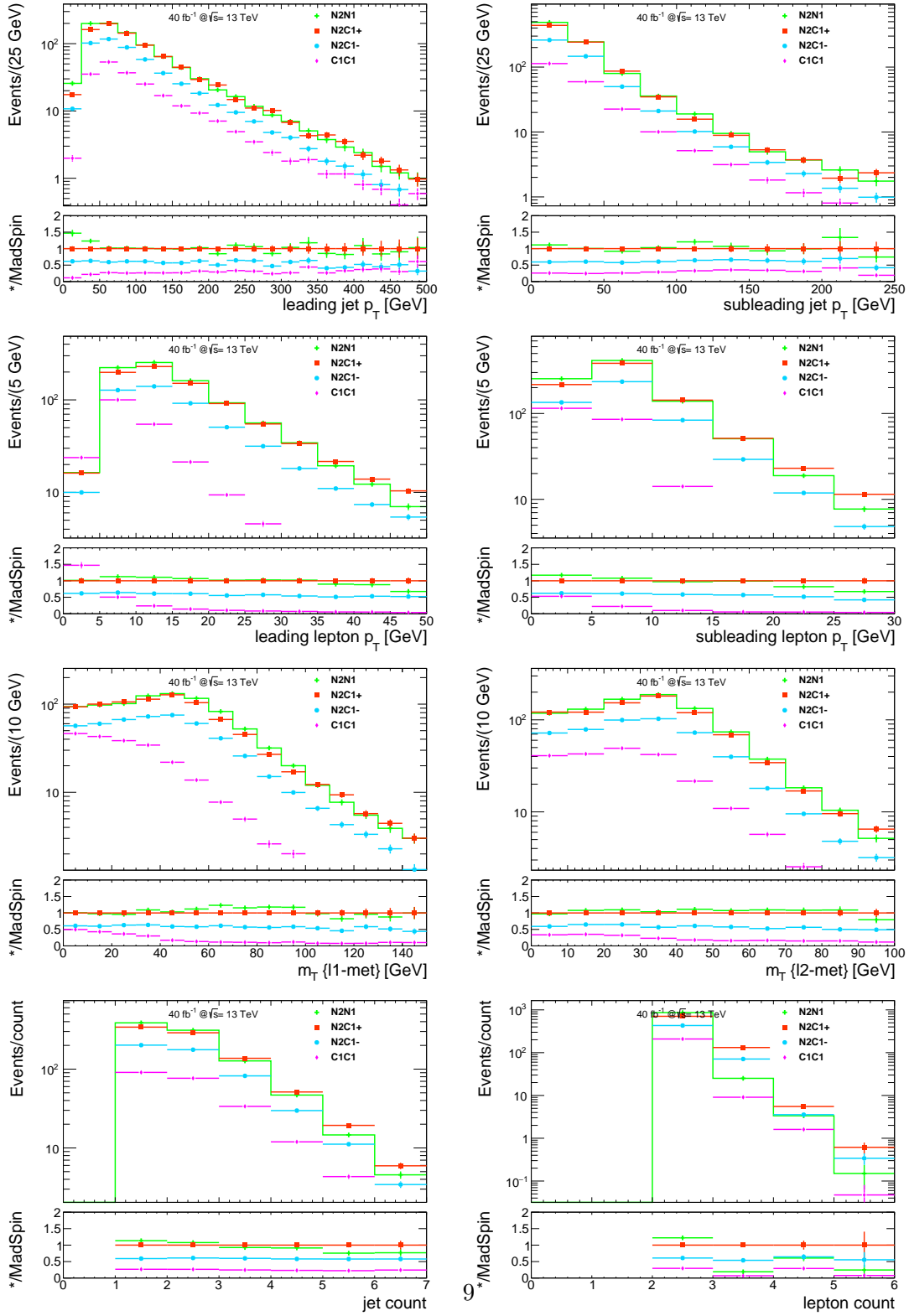


Figure 1: Kinematic distributions of signal samples

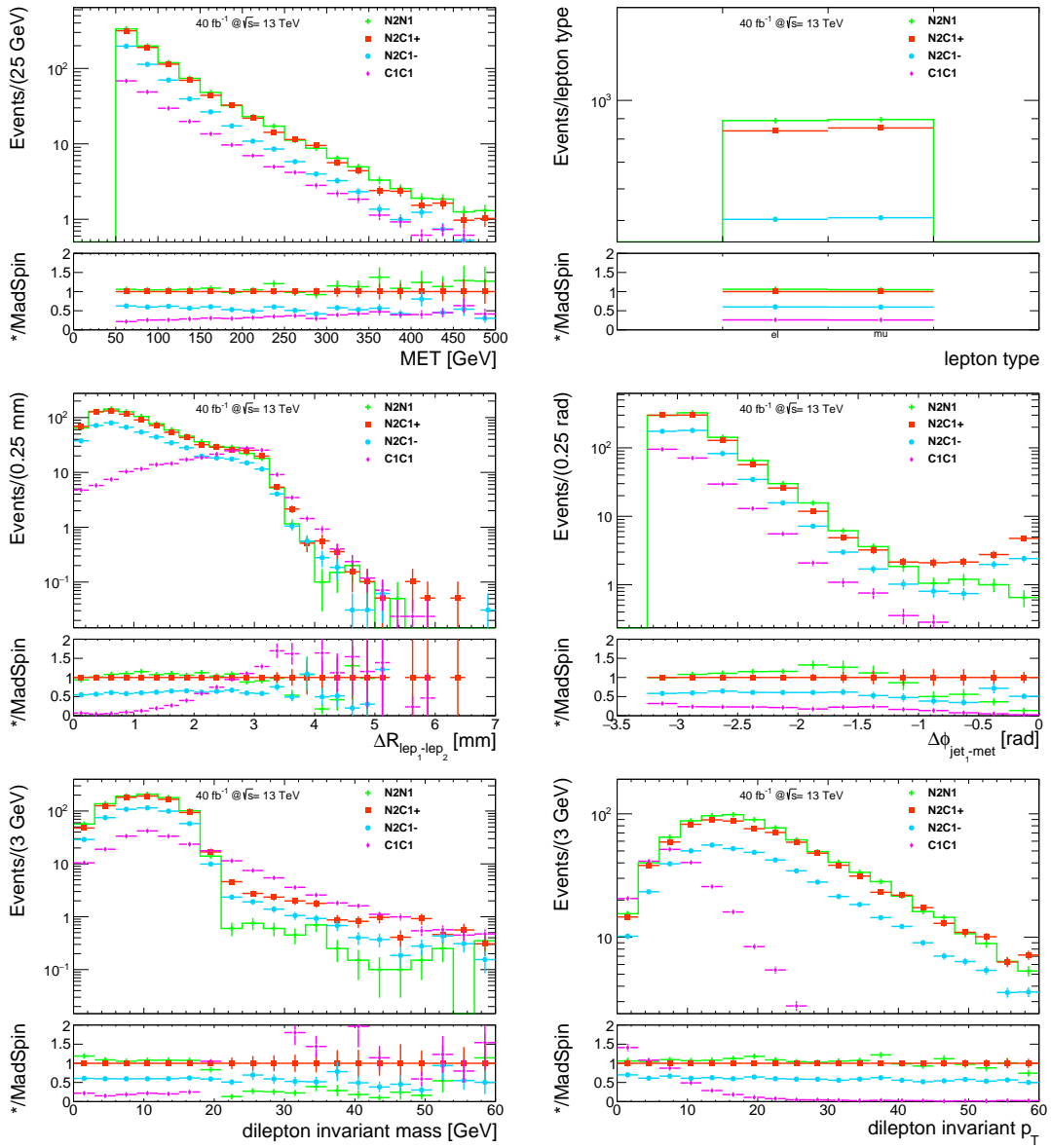


Figure 2: Kinematic distributions of signal samples

4.2 Triggers

4.2.1 MET Triggers

Inclusive met trigger efficiencies

4.2.2 Combined Triggers

Lepton plus jet plus met trigger efficiencies..

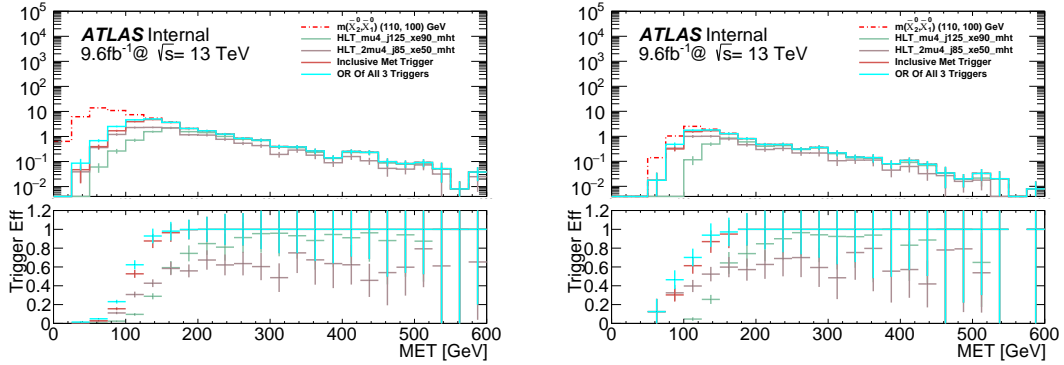


Figure 3: Trigger Efficiency as a function of MET after event preselection (left) and in a signal region similar to the analysis signal region (right)

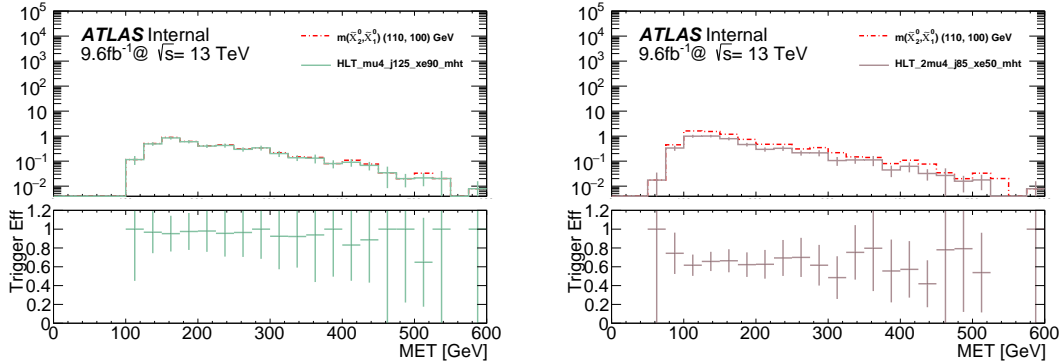


Figure 4: Trigger efficiency as a function of MET for the combined single muon trigger (left) and the combined dimuon trigger (right)

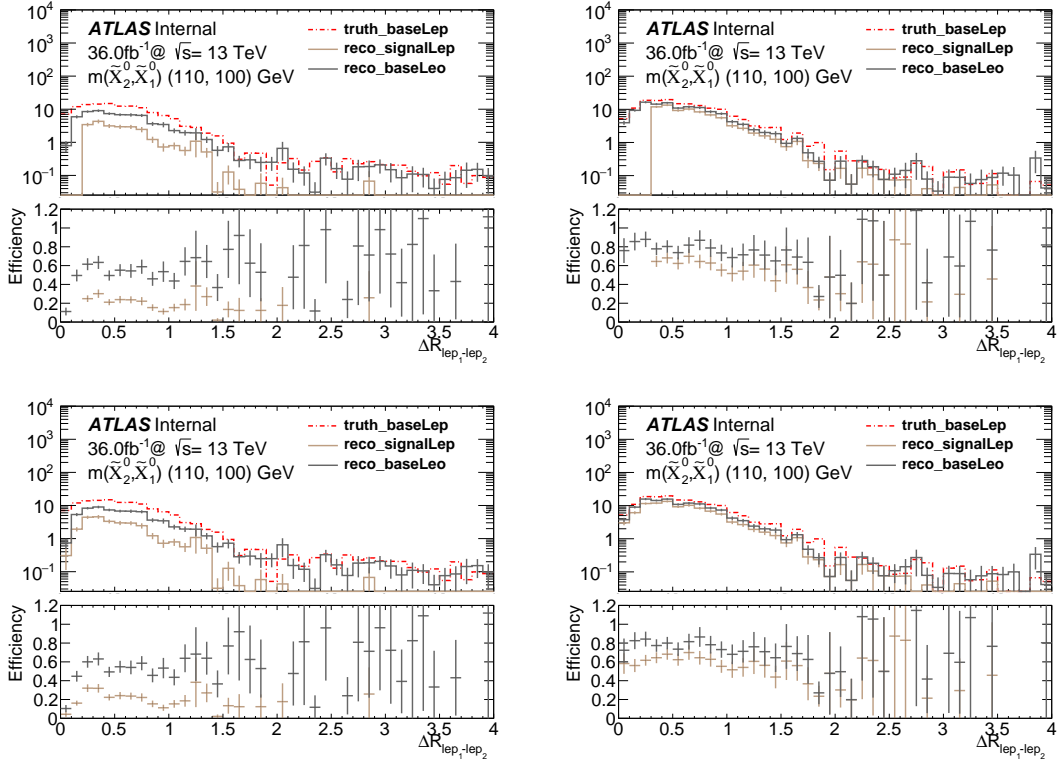


Figure 5: Dilepton ΔR distribution before LepIsoCorrection (top) and after LepIsoCorrection (bottom) for the ee -channel (left) and $\mu\mu$ -channel (right).

5 Event Selection and Signal Regions

Study signal MonteCarlos samples to understand the phenomenology of compressed higgsino and slepton production during and LHC collision and subsequent decay in the ALTAS detector. These studies inform our choices for signal region cuts for the slepton and higgsino searches.

5.1 Object Definitions

Electrons, muons, jets, photons, met, overlap removal, isolation for nearby leptons.. (lepton truth matching?)

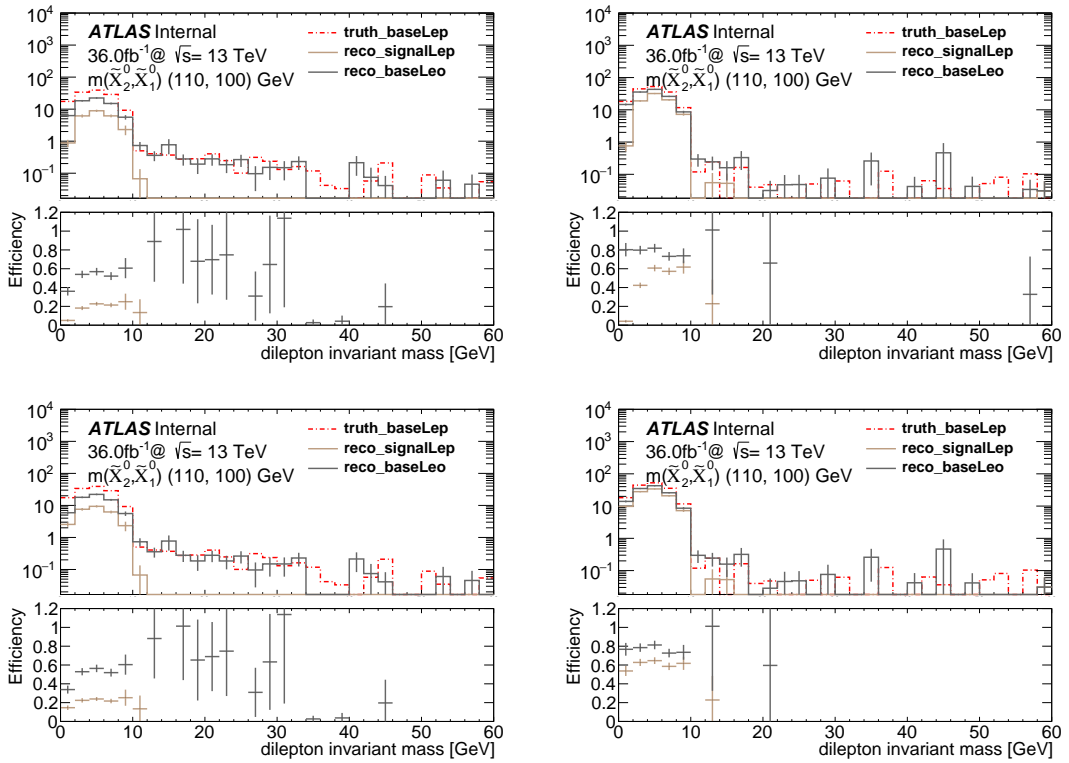


Figure 6: Dilepton invariant mass distribution before LepIsoCorrection (top) and after LepIsoCorrection (bottom) for the ee -channel (left) and $\mu\mu$ -channel (right).

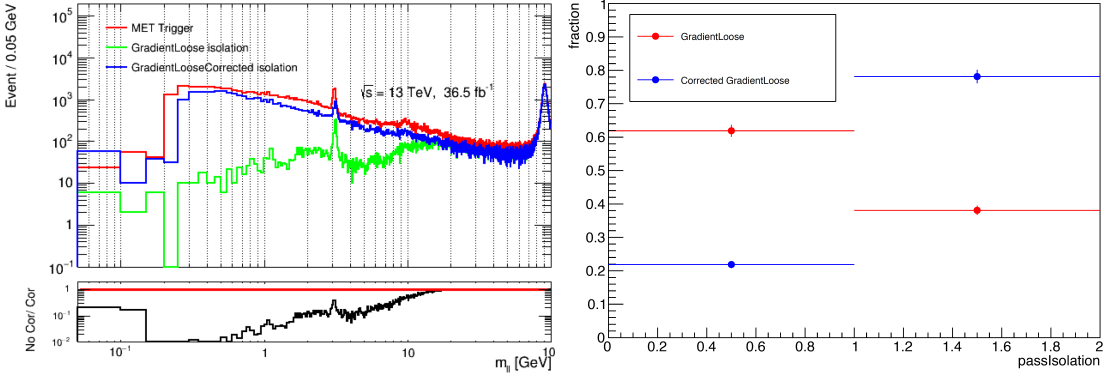


Figure 7: (left) Impact of the `NearbyLepIsoCorrection` tool on the efficiency of low-mass dilepton pairs in data. The data are shown in a region with $\Delta\phi(E_T^{\text{miss}}, p_t^{j1}) < 1.5$ to avoid the signal region. Events are triggered with the inclusive- E_T^{miss} trigger. The red trend shows events with two baseline leptons without applying any isolation; the green shows the impact of applying `GradientLoose` isolation; the blue shows the result of the `NearbyLepIsoCorrection` applied to the `GradientLoose` sample. (right) Impact of the correction on a Higgsino LSP signal sample with $\Delta m(\chi, \chi) = 3$ GeV.

5.2 Discriminating Variables

E_T^{miss} , d phi j-met, min d phi jets-met, $p_T(j_i)$, Number of b -tagged jets $N_{b-\text{jets}}$
 Same flavour lepton pair with opposite charge, $\Delta R_{\ell\ell}$, $m_{\ell\ell}$, $m_{T2}^{m_\chi}, m_T^{\ell_1}$, $E_T^{\text{miss}}/H_T^{\text{leptons}}$, $m_{\tau\tau}$

5.3 Signal Regions

5.3.1 Slepton Signal Regions

This signal region based on MT2 cuts

5.3.2 Higgsino Signal Regions

This signal region based on Mll cuts

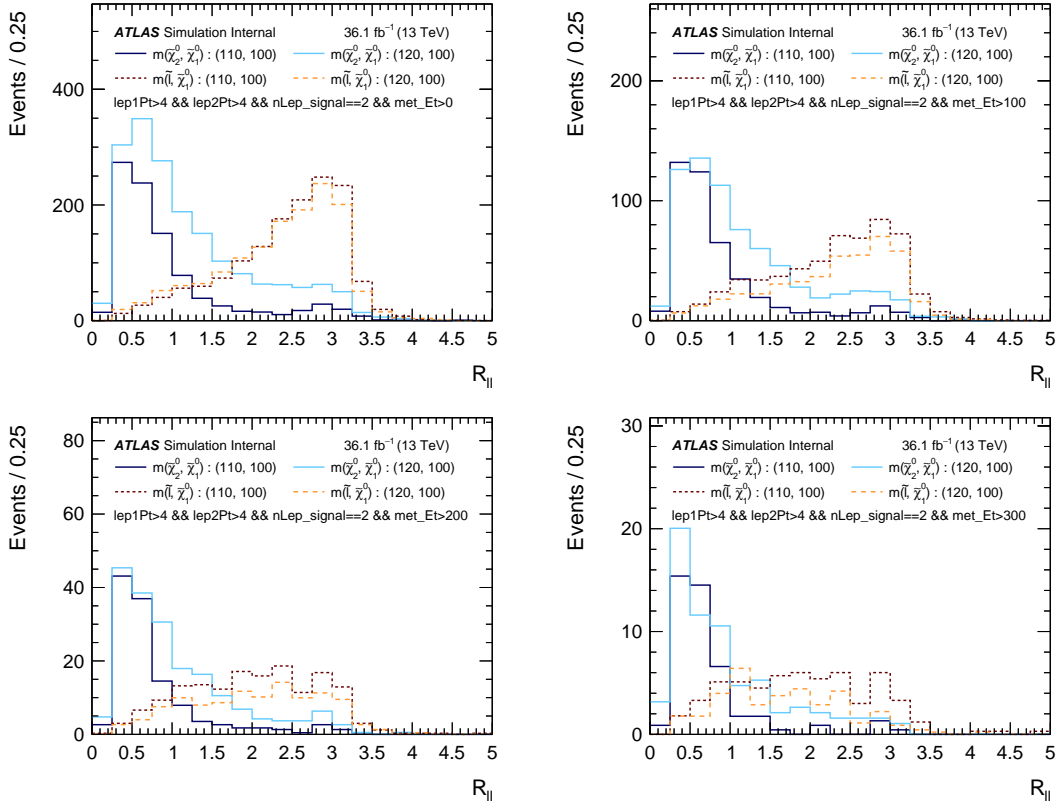


Figure 8: Comparison of Higgsino N2C1p (solid) and slepton (dashed) signals in the $R_{\ell\ell}$ variable for 10 GeV (dark) and 20 GeV (light) mass splittings. The E_T^{miss} here acts as a proxy for the boost of the system. Only a 2 signal lepton selection is applied.

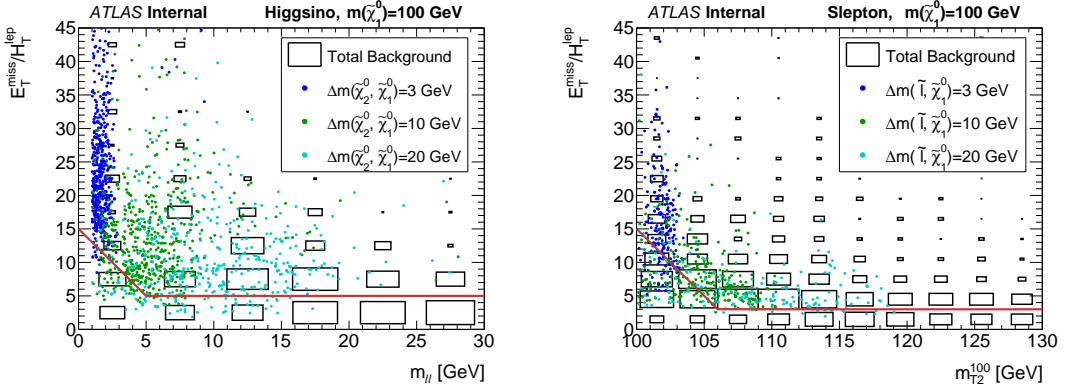


Figure 9: Distributions of $E_T^{\text{miss}}/H_T^{\text{leptons}}$ for the Higgsino (left) and Slepton (right) selections, after applying all signal region cuts except those on the $E_T^{\text{miss}}/H_T^{\text{leptons}}$, m_{ll} , and m_{T2} . The black dashed line indicates the cut applied in the signal region; events in the region below the black line are rejected.

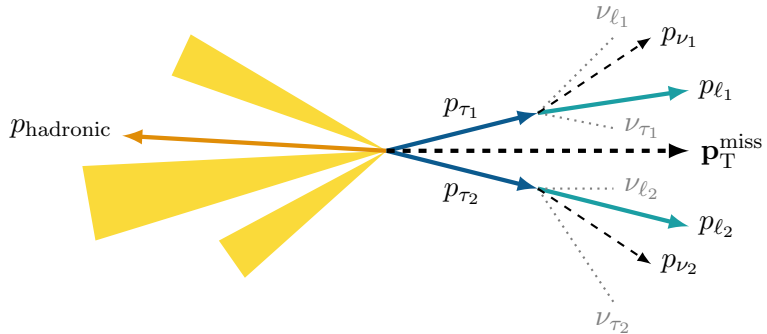


Figure 10: Schematic illustrating the fully leptonic ($Z \rightarrow \tau\tau$) + jets system motivating the construction of $m_{\tau\tau}$.

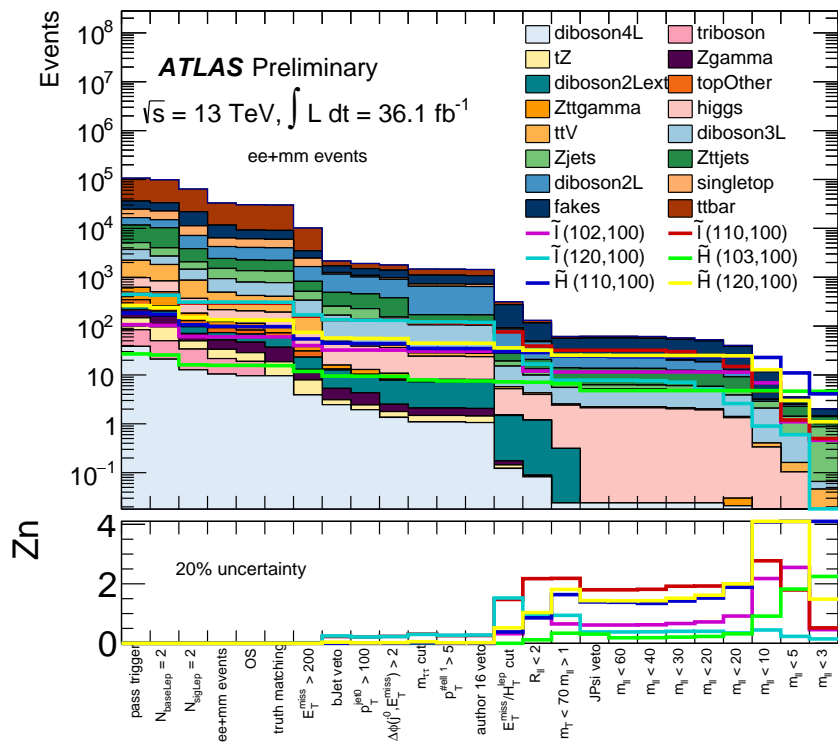


Figure 11: Non-normalized cutflow with significance plot, showing how the significance for signal improves as more cuts are added.

6 Fake Factor Method

Backgrounds to beyond Standard Model physics signals mostly come from Standard Model physics processes that produce the same physics signal that describes the new physics we are looking for. In that case the goal is the estimate the rate of the background process so that we can subtract it from the data and the signal we are looking for is all that remains. Another type of background can come from processes that should not produce the same final state as the signal process, and yet, because of mismeasurements inside the detector, can still mimic signal events. For low p_T dilepton signals, this background is a dominant background and primarily comes from W+jets events where one jets is misidentified as a lepton. The best estimate of this background comes from data because MC simulation does not model the detector shortcomings that lead to these mismeasurements very well. The "fake factor" method is a data driven approach to modeling backgrounds from particle misidentification in the detector. (Explain the layout of the rest of the chapter)

6.1 Introduction

Efficient lepton identification techniques make leptons are powerful discriminators in ATLAS physics searches with large background rejection and heavily suppressed QCD multijets. Jet suppression is very high in the range of lepton $p_T > 20\text{GeV}$ but degrades at lower lepton p_T . Sources of misidentified electrons are charged hadrons, where a hadronic jet fakes an electron, or photon conversions and heavy-flavor decays, where there is a true but non-prompt electron that is created inside the detector rather than at the primary vertex where true, prompt electrons are made.

**Make plot comparing production cross-sections, at least for W+jets and Higgsino/Slepton, and maybe even include other reducible background production cross-sections.

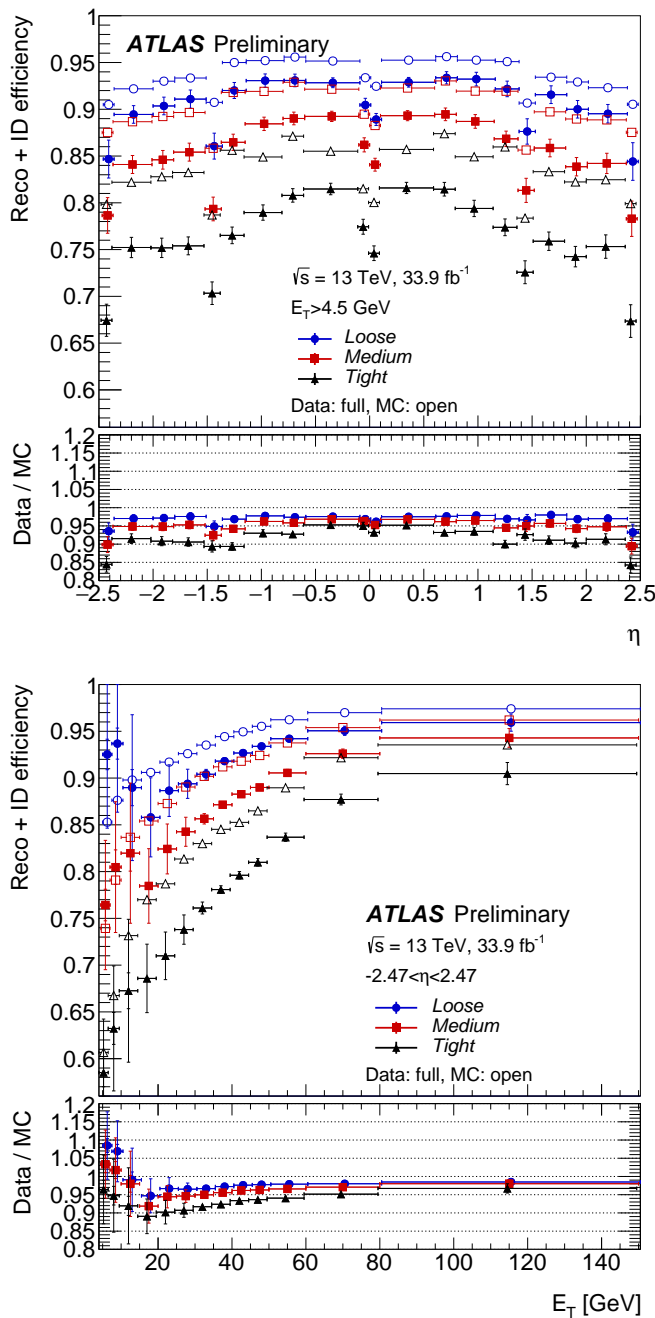


Figure 12: Electron identification efficiency

6.2 Fake Factor Method

Explain signal and control regions as well as fake factor measurement and application regions.

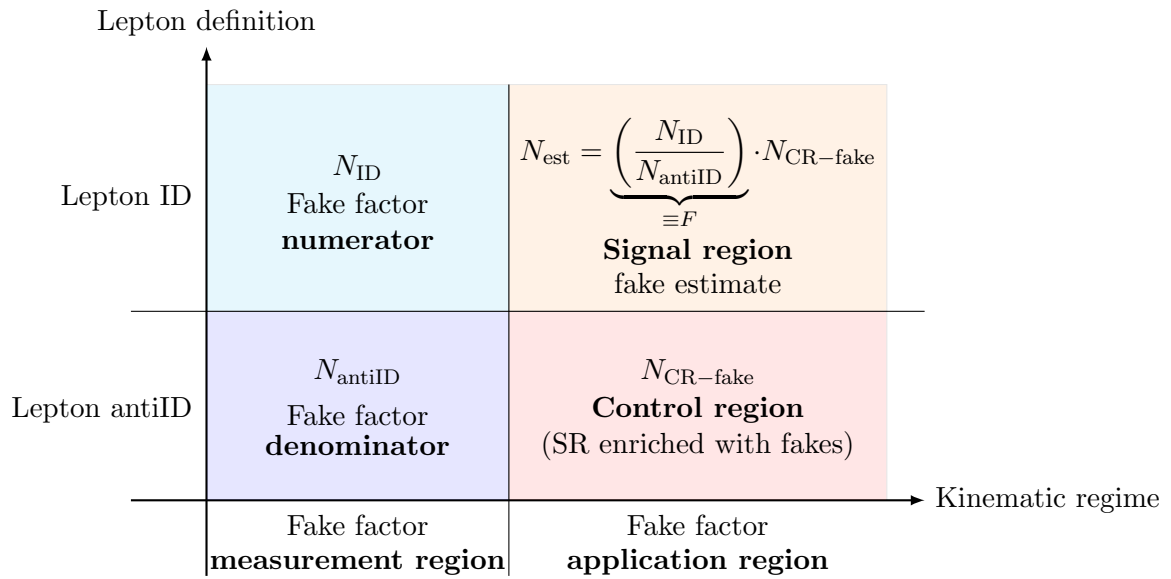


Figure 13: Schematic illustrating the fake factor method to estimate the fake lepton contribution in the signal region.

6.3 Fake Factor Method Applied to Low- p_T Di-lepton Events

6.3.1 Fake Factor Monte Carlo Studies

Trigger	Prescaled Luminosity [pb ⁻¹]	
	2015	2016
HLT_e5_lhvloose	0.1	0.1
HLT_e10_lhvloose_L1EM7	0.5	0.8
HLT_e15_lhvloose_L1EM13VH	5.5	9
HLT_e20_lhvloose	10	17
HLT_mu4	0.5	0.5
HLT_mu10	2.3	2.5
HLT_mu14	25	14
HLT_mu18	26	48

Table 1: Pre-scaled single-lepton triggers from 2015 and 2016 used to compute the lepton fake factors. The pre-scaled luminosities shown are taken from `LumiCalc`.

Electrons	Muons
$p_T > 4.5$ GeV	$p_T > 4$ GeV
$ \eta < 2.47$	$ \eta < 2.5$
$ z_0 \sin \theta < 0.5$ mm	$ z_0 \sin \theta < 0.5$ mm
Pass LooseAndBLayer identification	Pass Medium identification
(!Tight identification $ d_0/\sigma(d_0) > 5$!GradientLoose isolation)	($ d_0/\sigma(d_0) > 3$!FixedCutTightTrackOnly isolation)

Table 2: Summary of anti-ID lepton definitions.

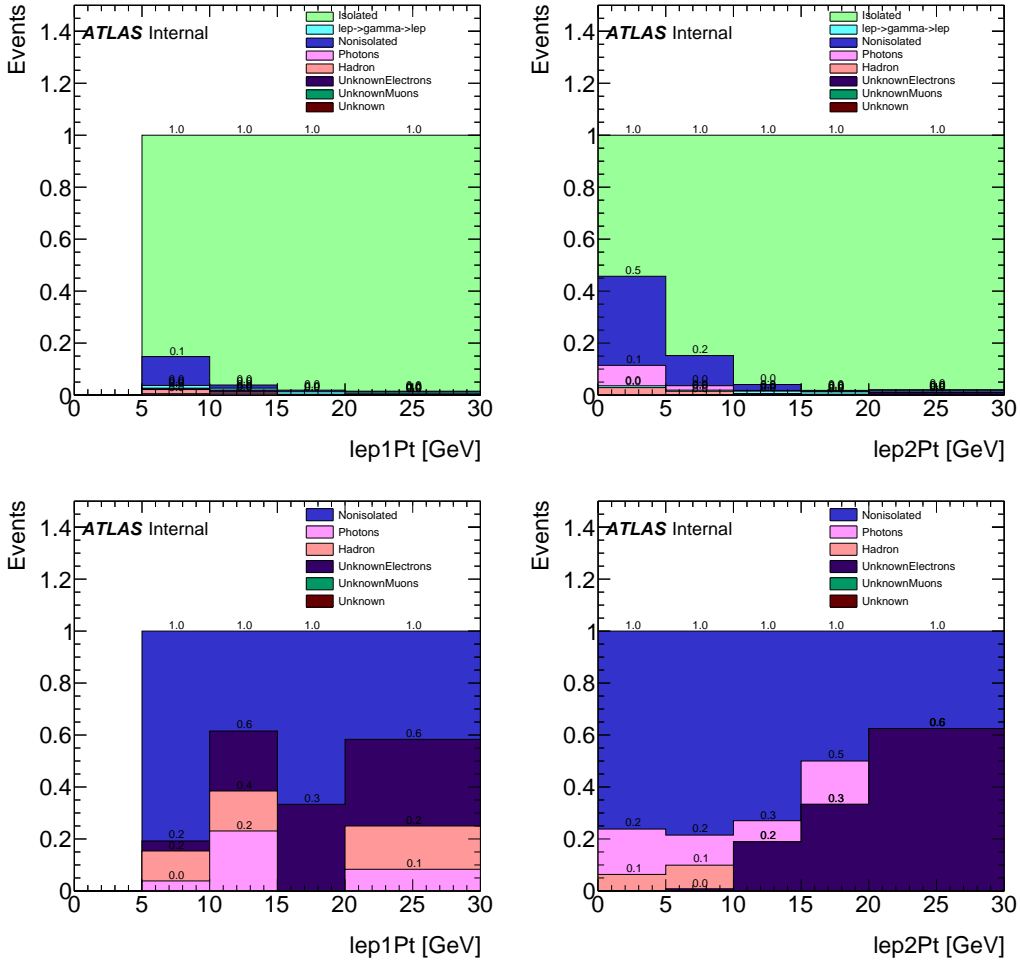


Figure 14: Fake lepton composition as a function of leading and subleading lepton p_T , with and without prompt (“Isolated” plus “le \rightarrow gamma \rightarrow lep”) leptons, for opposite sign electron pairs in the signal region.

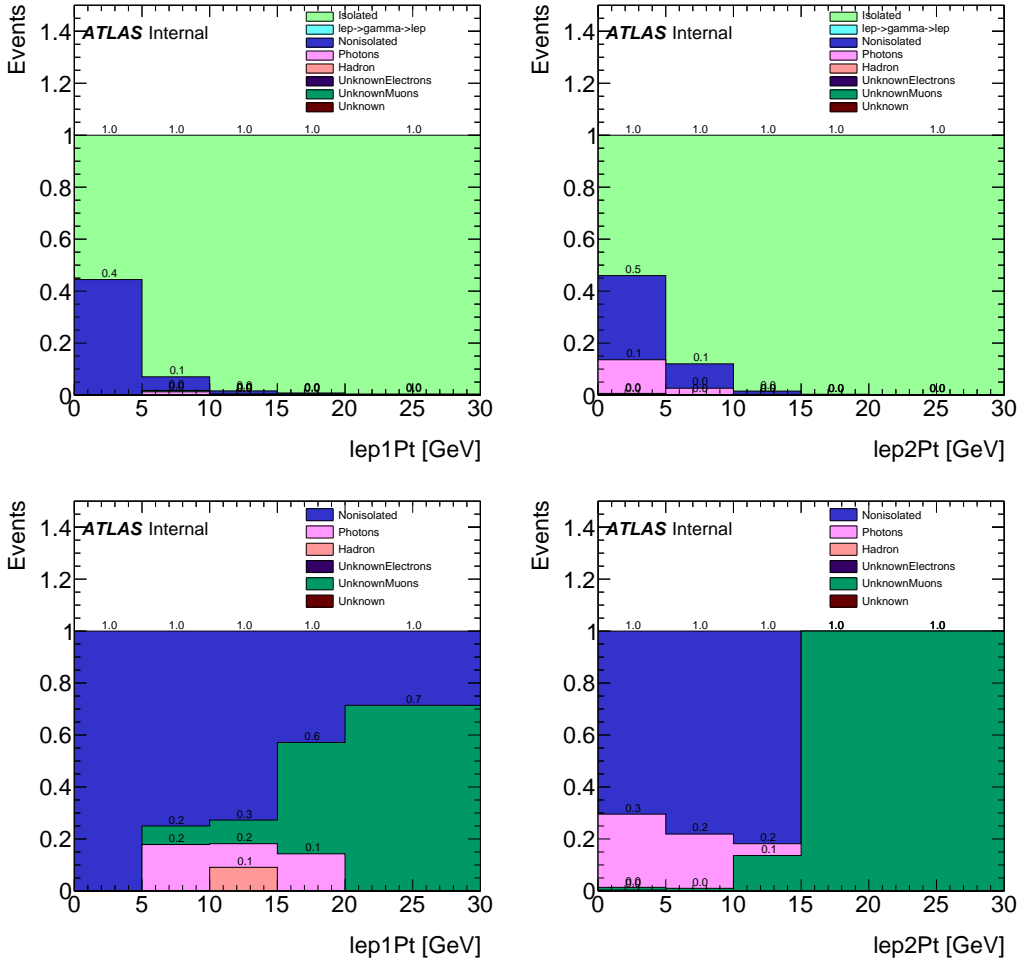


Figure 15: Fake lepton composition as a function of leading and subleading lepton p_T , with and without prompt (“Isolated” plus “ $\text{lep} \rightarrow \text{gamma} \rightarrow \text{lep}$ ”) leptons, for opposite sign muon pairs in the signal region.

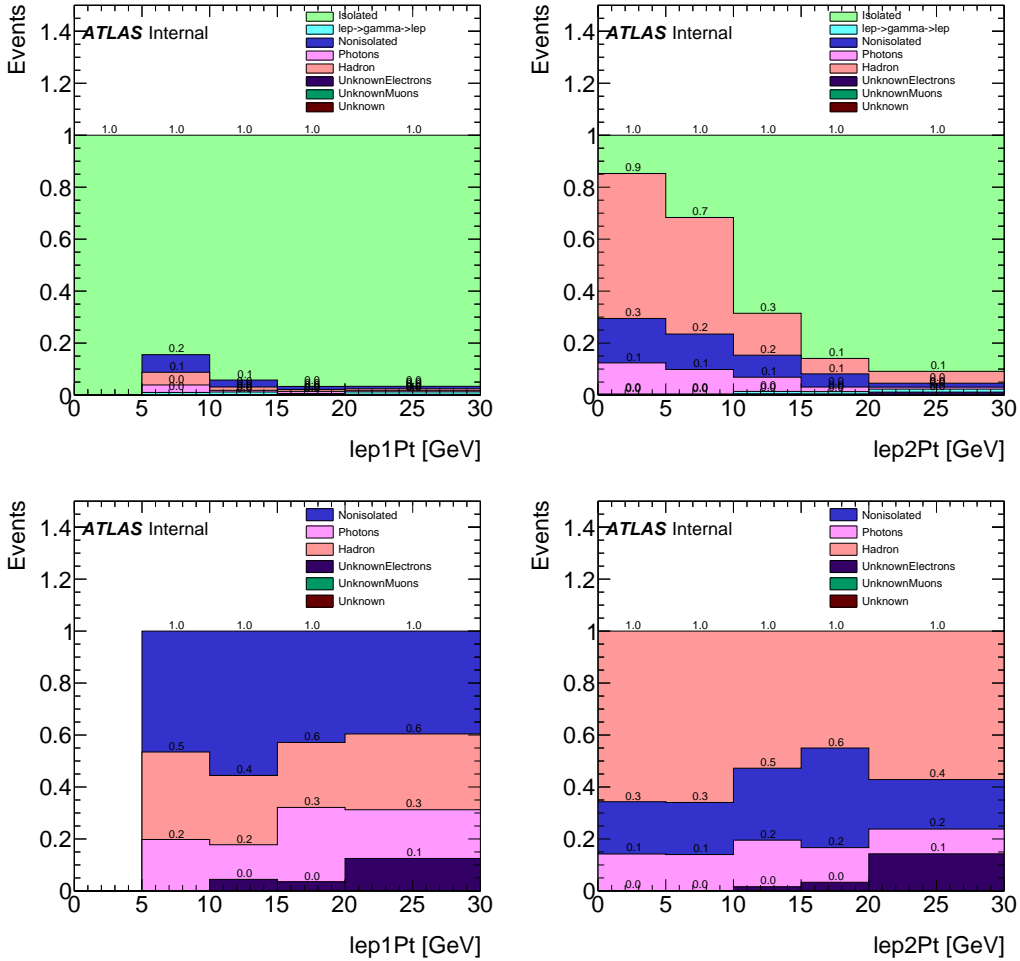


Figure 16: Fake lepton composition as a function of leading and subleading lepton p_T , with and without prompt (“Isolated” plus “ $\text{lep} \rightarrow \text{gamma} \rightarrow \text{lep}$ ”) leptons, for opposite sign electron pairs in the fake lepton control region.

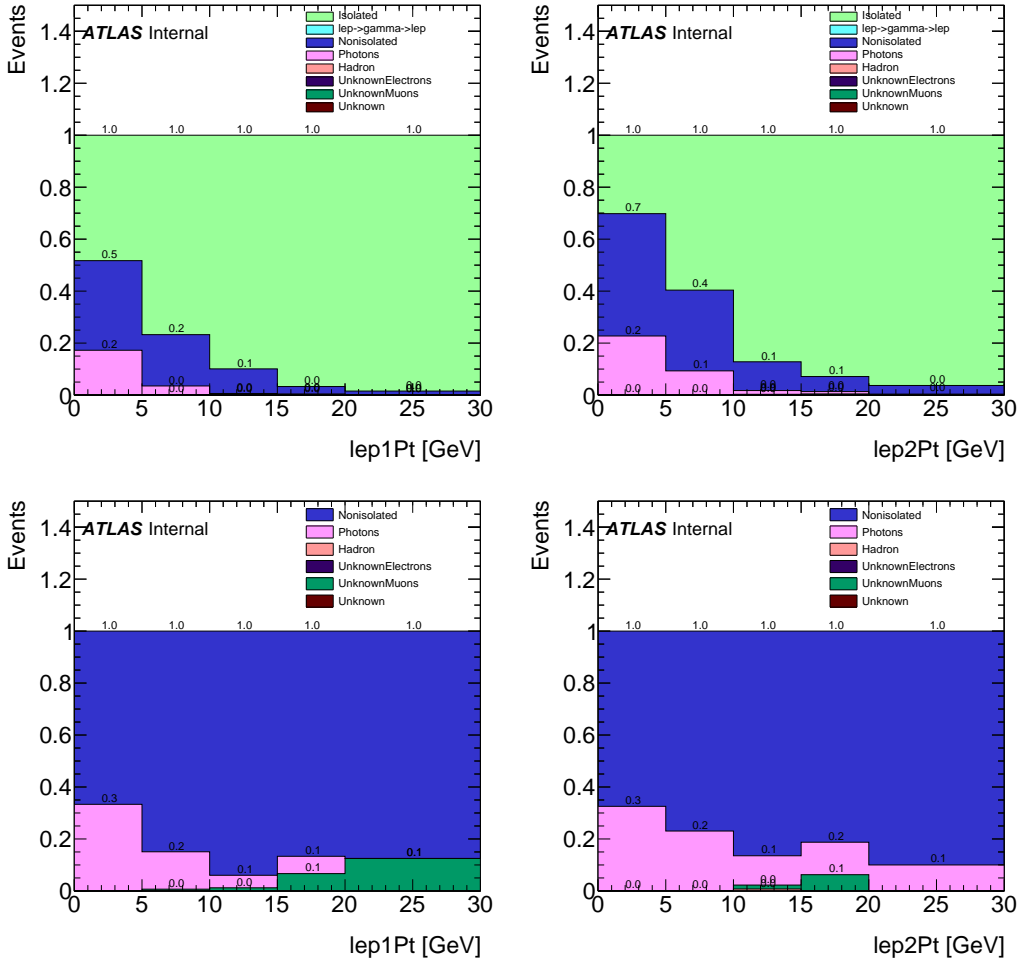


Figure 17: Fake lepton composition as a function of leading and subleading lepton p_T , with and without prompt (“Isolated” plus “ $\text{lep} \rightarrow \text{gamma} \rightarrow \text{lep}$ ”) leptons, for opposite sign muon pairs in the fake lepton control region.

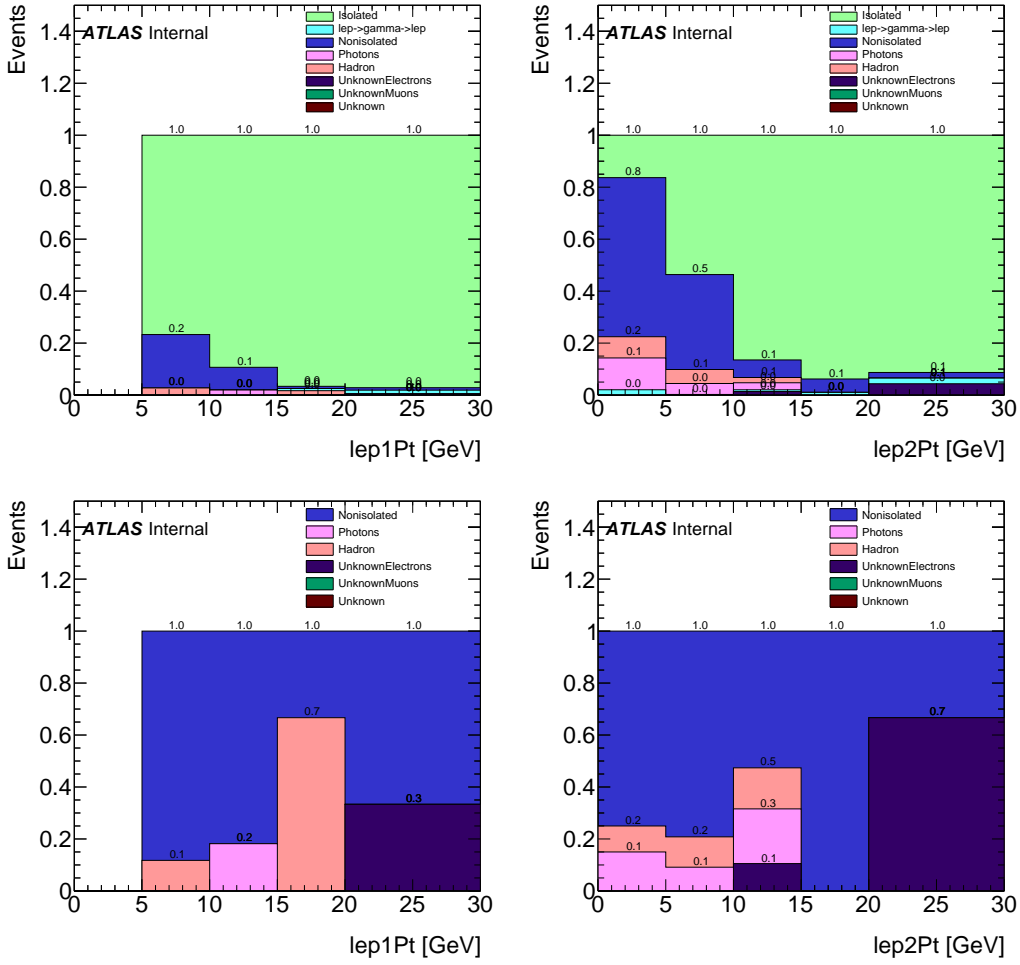


Figure 18: Fake lepton composition as a function of leading and subleading lepton p_T , with and without prompt (“Isolated” plus “le \rightarrow gamma \rightarrow lep”) leptons, for same sign electron pairs in the signal region.

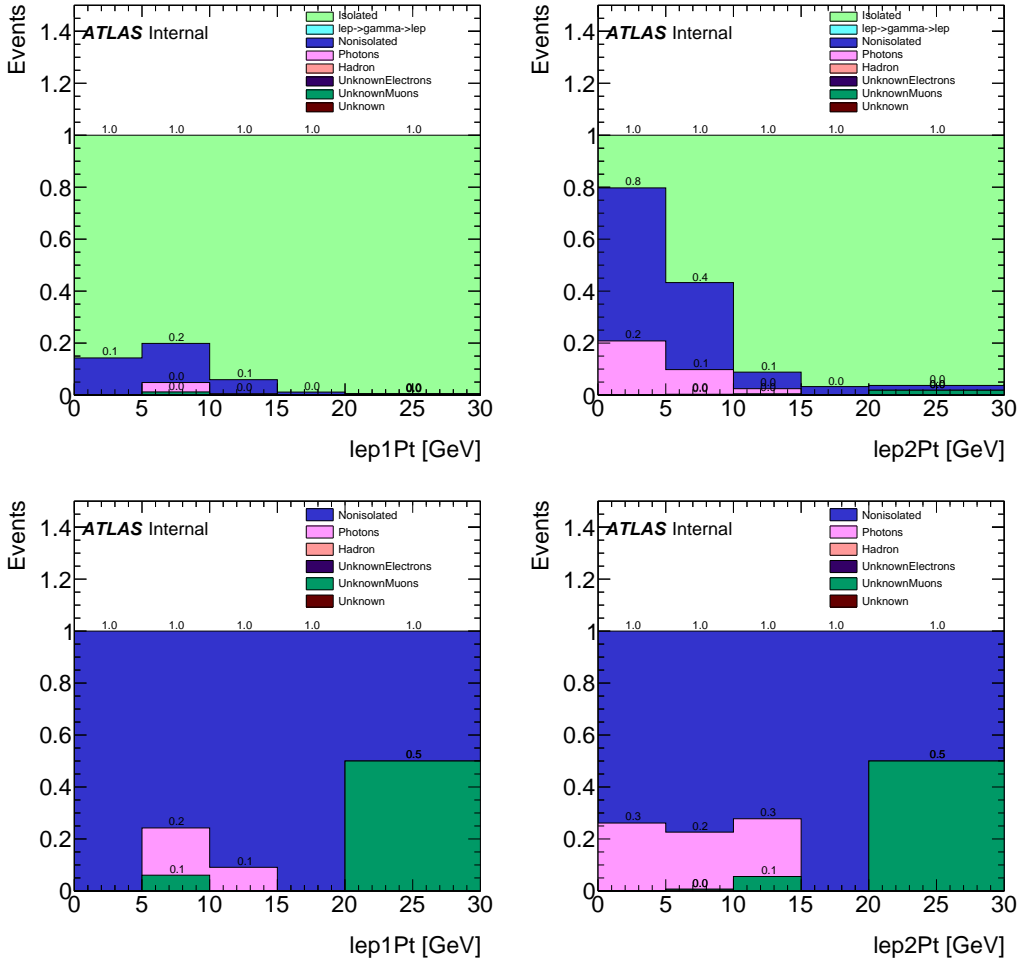


Figure 19: Fake lepton composition as a function of leading and subleading lepton p_T , with and without prompt (“Isolated” plus “ $\text{lep} \rightarrow \text{gamma} \rightarrow \text{lep}$ ”) leptons, for same sign muon pairs in the signal region.

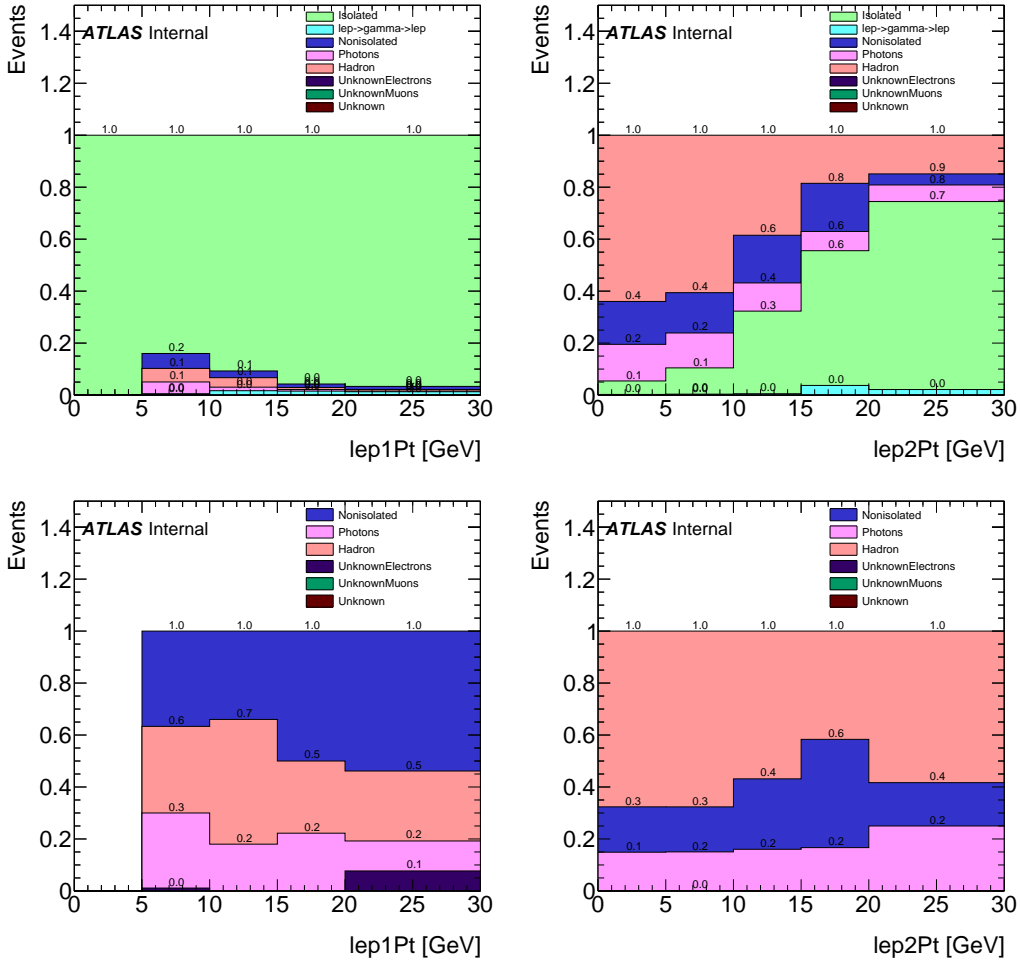


Figure 20: Fake lepton composition as a function of leading and subleading lepton p_T , with and without prompt (“Isolated” plus “ $\text{lep} \rightarrow \gamma \rightarrow \text{lep}$ ”) leptons, for same sign electron pairs in the fake lepton control region.

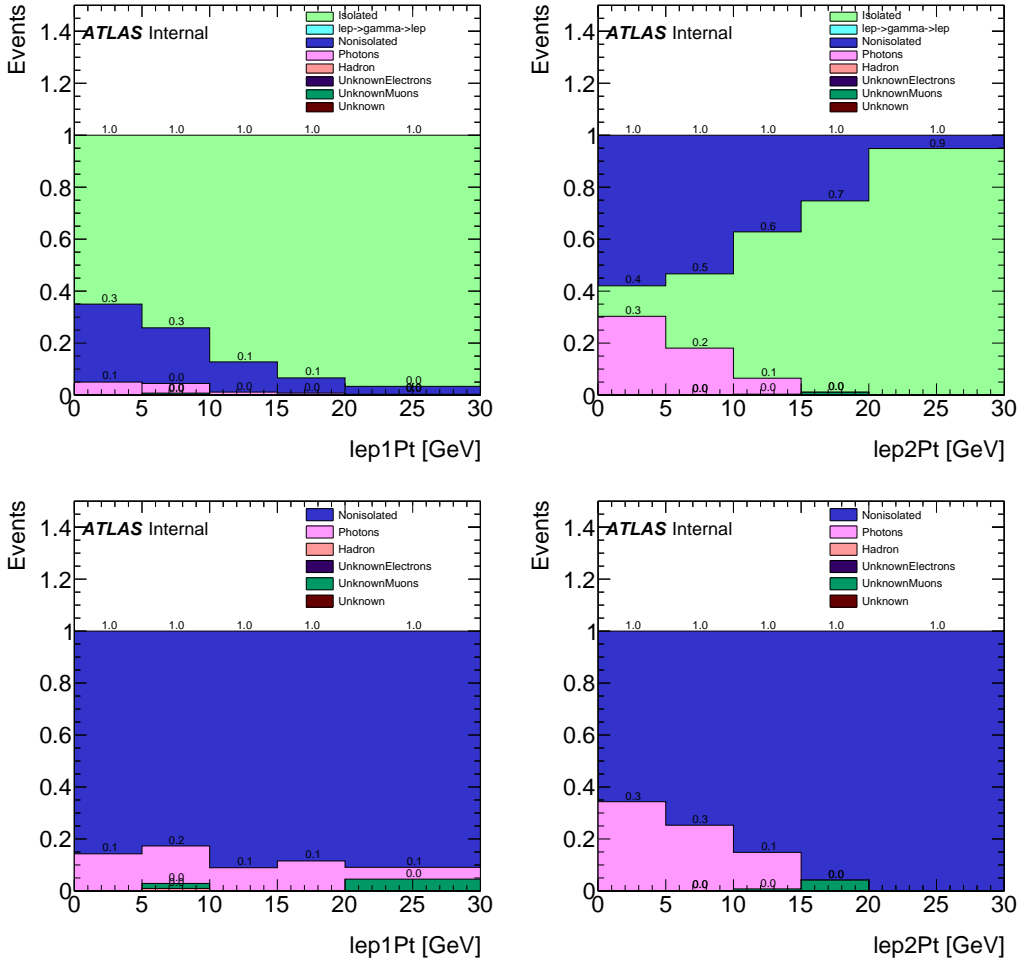


Figure 21: Fake lepton composition as a function of leading and subleading lepton p_T , with and without prompt (“Isolated” plus “le \rightarrow gamma \rightarrow le \rightarrow ”) leptons, for same sign muon pairs in the fake lepton control region.

6.3.2 Electron Fake Factors

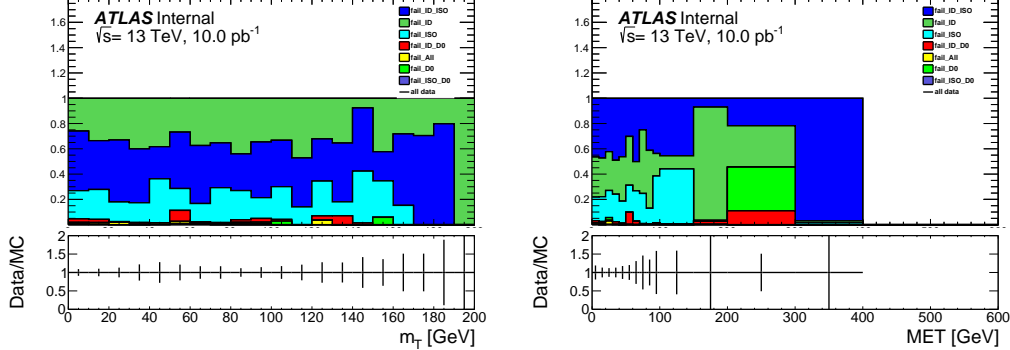


Figure 22: Fake electron composition as a function of m_T for events in the full m_T range (left) and as a function of E_T^{miss} (top) for events in the range $m_T < 40$ GeV.

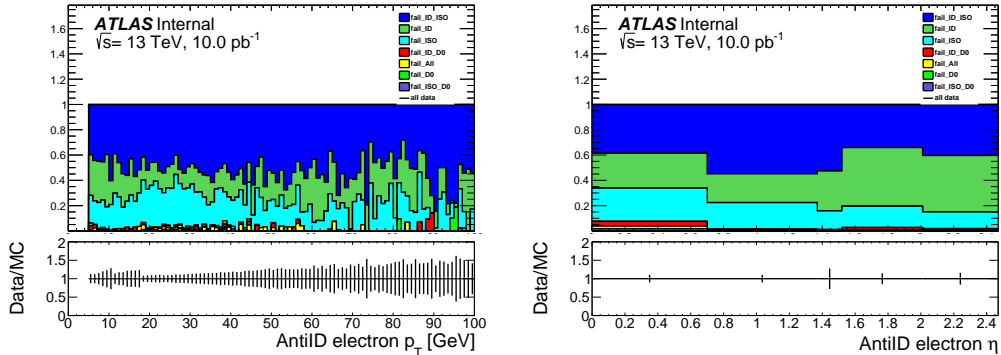


Figure 23: Fake electron composition as a function of denominator electron p_T (left) and as a function of denominator electron η (top) for events with $m_T < 40$ GeV.

The fake factors are computed from events with $m_T < 40$ GeV, using the distributions in Fig. 25, as:

$$F(p_T) = \frac{\text{Numerator}_{\text{data}} - \text{Numerator}_{\text{MC}}}{\text{Denominator}_{\text{data}} - \text{Denominator}_{\text{MC}}} \quad (2)$$

Electron fake factors show the largest dependence on electron p_T , but also display a dependence on the leading jet p_T , which is evident in Fig. 27 that shows electron fake factors as a function of electron p_T and leading jet p_T separately. Given this trend, and the fact that all signal regions used in this analysis require a hard jet with p_T greater than 100 GeV, we design the fake factor measurement region to also require a hard jet of

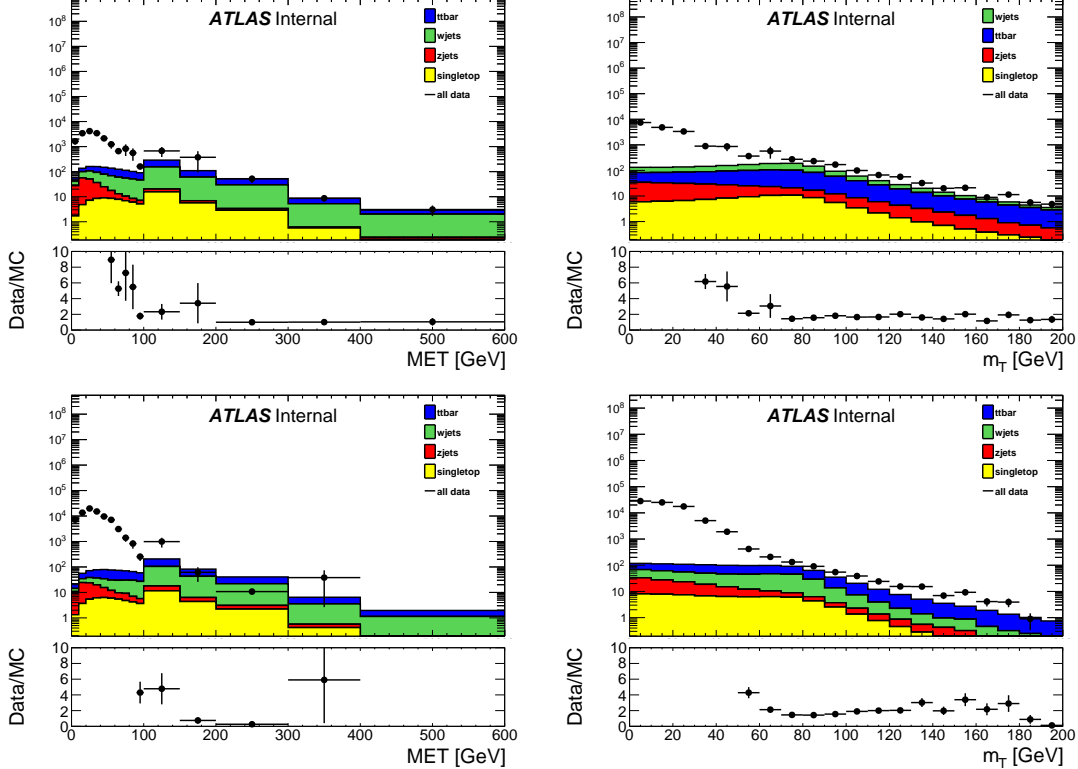


Figure 24: The E_T^{miss} (left) and m_T (right) distributions for numerator (top) and denominator (bottom) electrons in the prescaled single-lepton-trigger sample. MC has been scaled to the data in the $E_T^{\text{miss}} > 200$ GeV region.

el trigger	p_T range [GeV]
HLT_e5_lvloose	5–11
HLT_e10_lvloose_L1EM7	11–18
HLT_e15_lvloose_L1EM13VH	18–23
HLT_e20_lvloose	> 23

Table 3: Single-Electron triggers used for fake factor computation and their corresponding p_T range.

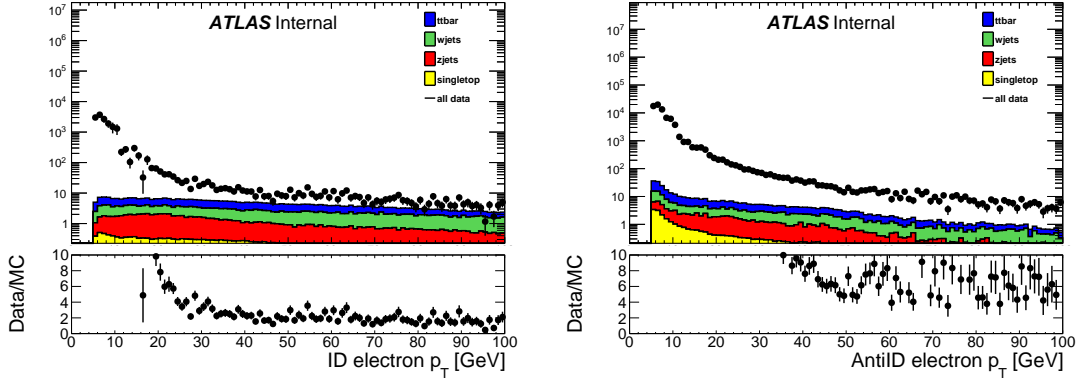


Figure 25: Electron p_T for numerator (left) and denominator (right) objects in the prescaled single-lepton-trigger sample for events with $m_T < 40\text{GeV}$. MC has been scaled to the data in the $E_T^{\text{miss}} > 200\text{ GeV}$ region.

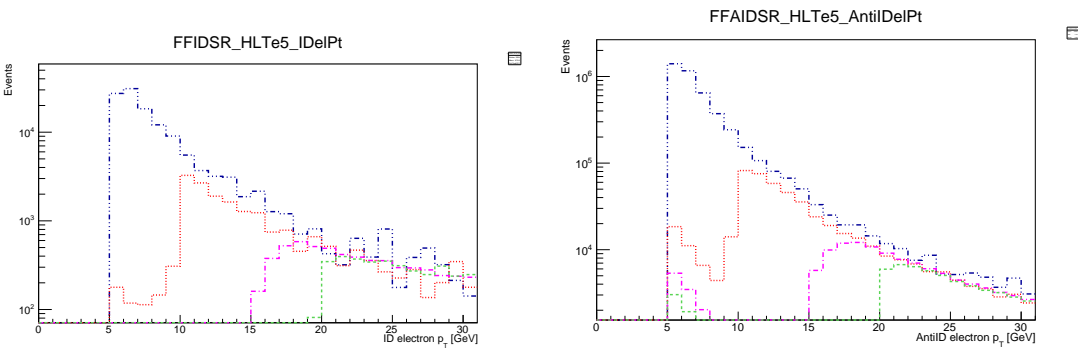


Figure 26: The numerator electron (left) and denominator electron (right) p_T distributions for prescaled single-lepton-trigger, normalized to 1 pb^{-1} . Blue curve: HLT_e5_lvhloose, red curve: HLT_e10_lvhloose_L1EM7, purple curve: HLT_e15_lvhloose_L1EM13, green curve: HLT_e20_lvhloose.

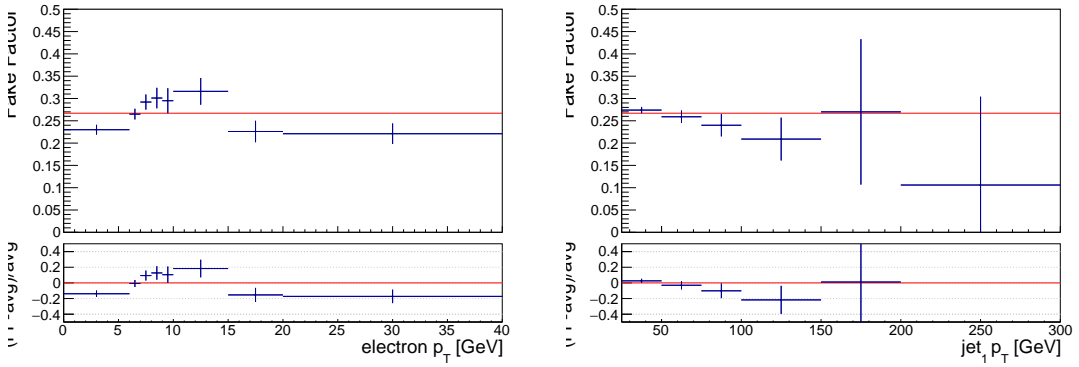


Figure 27: Electron fake factors *before* requiring a hard jet of $p_T > 100$ GeV, computed from single-electron prescaled triggers as a function of electron p_T (left) and leading jet p_T (right). Fake factors for electron p_T 4.5 – 5 GeV are taken to be the same as electron p_T 5 – 6 GeV. A red line denotes the average electron fake factor over all electron p_T of 0.267.

p_T greater than 100 GeV. Fake factors as a function of other kinematic variables are also studied as a cross-check and for understanding systematic uncertainties.

Final fake factors computed as a function of electron p_T are shown in Fig. 28a. In addition, fake factors as functions of other variables are also inspected to check for significant trends:

- the dependence of the fake factors on $|\eta|$ is shown in Fig. 28b,
- fake factors as a function of leading jet p_T and $\Delta\phi_{jet-E_T^{\text{miss}}}$ are shown in Fig. 29,
- fake factors as a function of jet multiplicity and b -jet multiplicity are shown in Fig. 30,
- fake factors as a function of pile up variables, such as average interaction per bunch crossing and number of primary vertices, are also shown in Fig. 31.

The relative uncertainties on the final electron fake factors versus electron p_T are shown in Fig. 32.

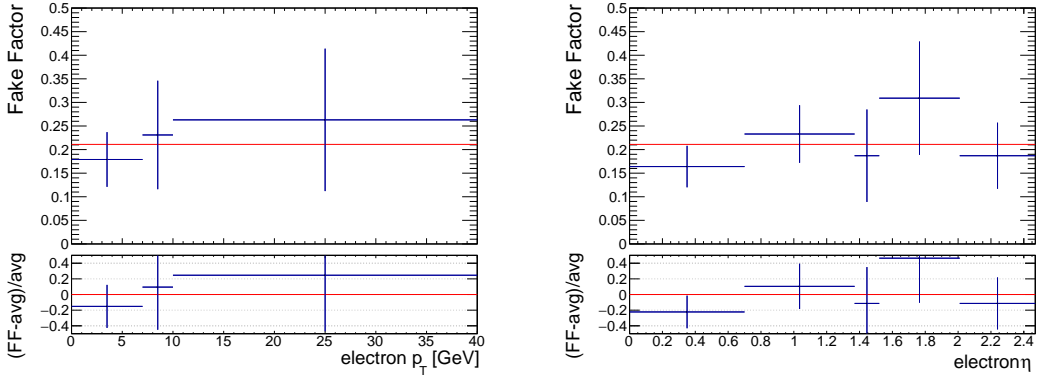


Figure 28: Electron fake factors computed from single-electron prescaled triggers as a function of electron p_T (left) and electron η (right) in the kinematic region with leading jet $p_T > 100\text{GeV}$. Fake factors for electron p_T 4.5 – 5 GeV are taken to be the same as electron p_T 5 – 6 GeV. A red line denotes the average electron fake factor over all electron p_T of 0.211.

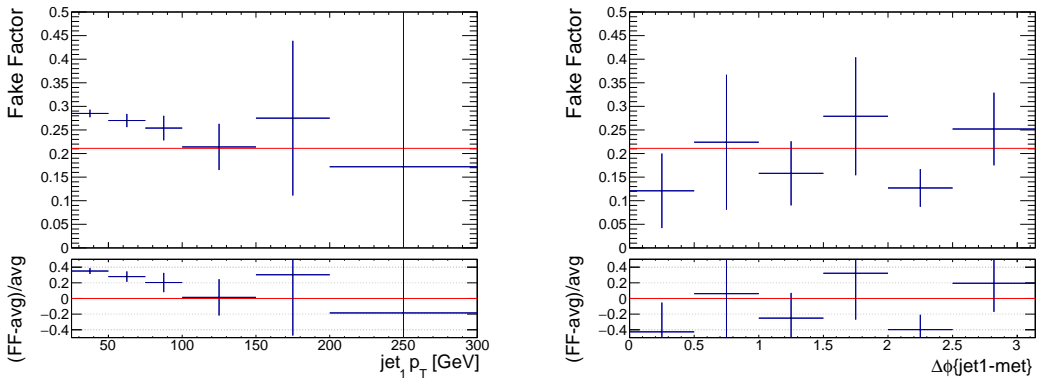


Figure 29: Electron fake factors computed from single-electron prescaled triggers as a function of leading jet p_T (left) and $\Delta\phi_{jet-E_T^{\text{miss}}}$ (right). A red line denotes the average electron fake factor over all electron p_T of 0.211.

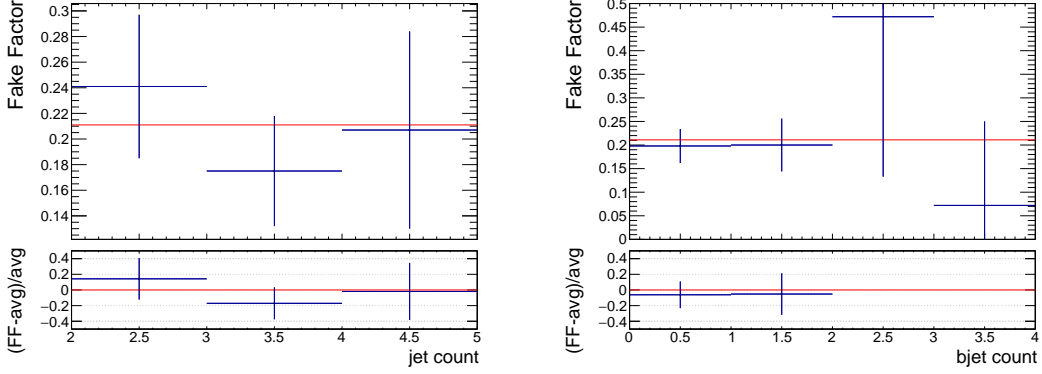


Figure 30: Electron fake factors computed from single-electron prescaled triggers as a function of the jet multiplicity (left) and the b -jet multiplicity (right). A red line denotes the average electron fake factor over all electron p_T of 0.211.

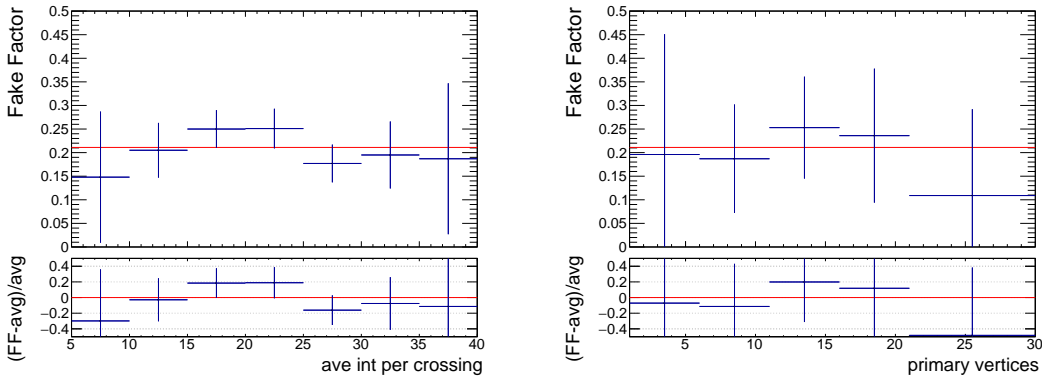


Figure 31: Electron fake factors computed from single-electron prescaled triggers as a function of the average interaction per bunch crossing (left) and the number of primary vertices (right). A red line denotes the average electron fake factor over all electron p_T of 0.211.

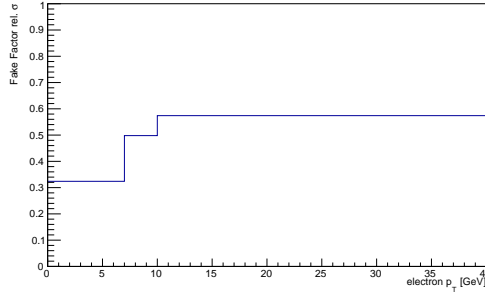


Figure 32: Relative uncertainties on electron fake factors binned electron p_T .

6.3.3 Muon Fake Factors

The muon fake factors are derived in a very similar way as the electron fake factors. The “numerator” muons, also called th ID muons, are the same as signal muons as defined in Section ??, which are baseline muons that are required to pass `FixedCutTightTrackOnly` isolation and $|d_0/\sigma(d_0)| < 3.0$. ”Denominator” muons, also called anti-ID muons, are defined as baseline muons that fail at least one of the signal muon requirements, i.e. they are required to fail either the `FixedCutTightTrackOnly` isolation or $|d_0/\sigma(d_0)| < 3.0$. All numerators and denominators are required to pass the $|z_0 \sin \theta| < 0.5$ mm requirement to reduce the impact of pileup. One notable difference with respect to the signal muon requirements is that the muon-jet overlap removal is relaxed when performing the fake factor measurement¹.

The decomposition of denominator muons in all events according to which ID criteria or combination of ID criteria failed is shown in Fig 33 and Fig 34. The m_T distribution of this decomposition in Fig 33 is plotted over the entire m_T range, while the E_T^{miss} distribution in Fig 33 and the p_T and η distributions in Fig 34 are all shown for $m_T < 40$ GeV. Note that these distributions are separated into categories: one for events with exactly zero b -jets, and another for events with one or more b -jets.

Both data and MC contributions to the numerator and denominator samples in the single-muon trigger sample are normalized to 10 pb^{-1} , to remove the effects of the prescales in the data. The MC is then re-scaled to the data in events with $E_T^{\text{miss}} > 200$ GeV, a kinematic region expected to be pure in prompt leptons. For events with exactly 0 b -jets, the MC re-scaling factor for numerator muons is 1.01 ± 0.13 , for denominator muons it is 1.20 ± 0.29 . For events with one or more b -jets, the MC re-scaling factor for numerator muons is 1.24 ± 0.20 , for denominator muons it is 7.34 ± 5.00 . If instead, the MC is re-scaled

¹This enhances the statistics used for deriving the fake factors, and is motivated by the observation that the muon-jet overlap removal is primarily designed to reduce the number of heavy flavor decays which are inadvertently being classified as signal muons, i.e. a sample of events that is interesting to keep for a fake measurement.

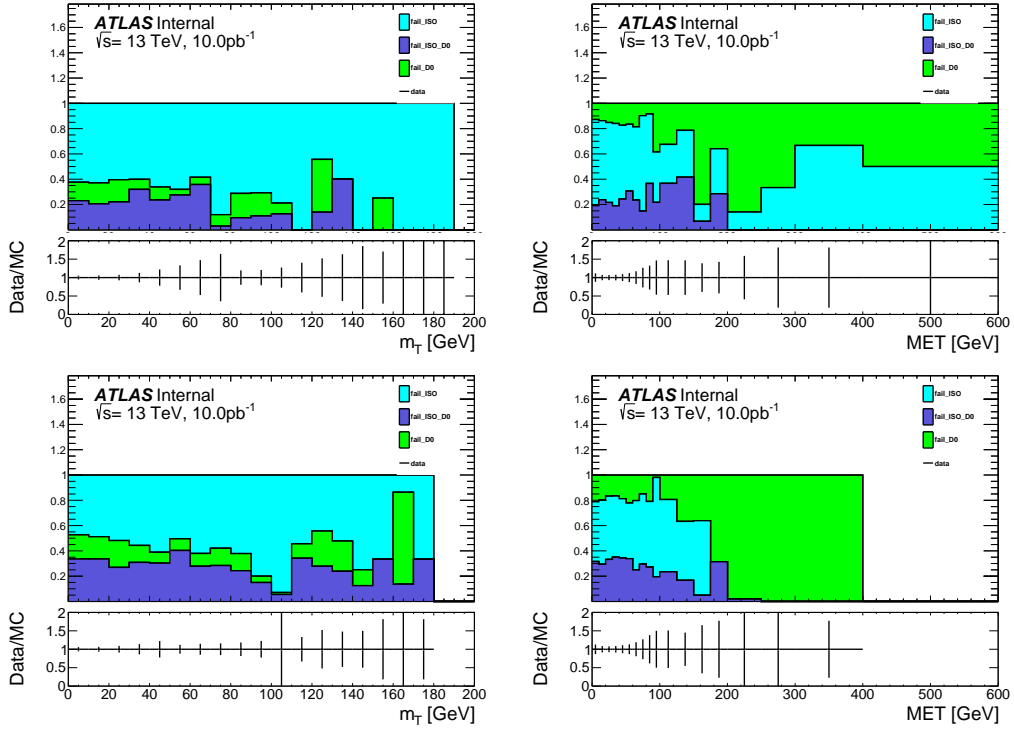


Figure 33: Anti-ID muon composition in events with exactly zero b -jets (top) and one or more b -jets (bottom) as a function of m_T (left) and as a function of E_T^{miss} (right). The E_T^{miss} distribution corresponds to events with $m_T < 40 \text{ GeV}$.

to match the data for events with $m_T > 100 \text{ GeV}$, a region that should also be pure in prompt leptons, the re-scaling factors for events with exactly 0 b -jets are 2.37 ± 0.10 for numerator muons and 11.68 ± 2.28 for denominator muons; events with one or more b -jets have re-scale factors 1.60 ± 0.06 for numerator muons and 10.41 ± 6.34 for denominator muons. The re-scaling factors vary significantly between the two methods but the fake factors themselves exhibit small changes between the two methods and can be used as a systematic uncertainty.

Distributions of E_T^{miss} and m_T for numerator and denominator muons for events with exactly zero b -jets are shown in Fig. 35, and for events with one or more b -jets in Fig. 36. Muon p_T distributions for events with exactly zero b -jet are shown in Fig. 37, and for events with one or more b -jets in Fig. 38.

The fake factors are computed using events with $m_T < 40 \text{ GeV}$, using the distribution in Figs. 37 and 38, as

$$F(p_T) = \frac{\text{Numerator}_{\text{data}} - \text{Numerator}_{\text{MC}}}{\text{Denominator}_{\text{data}} - \text{Denominator}_{\text{MC}}} \quad (3)$$

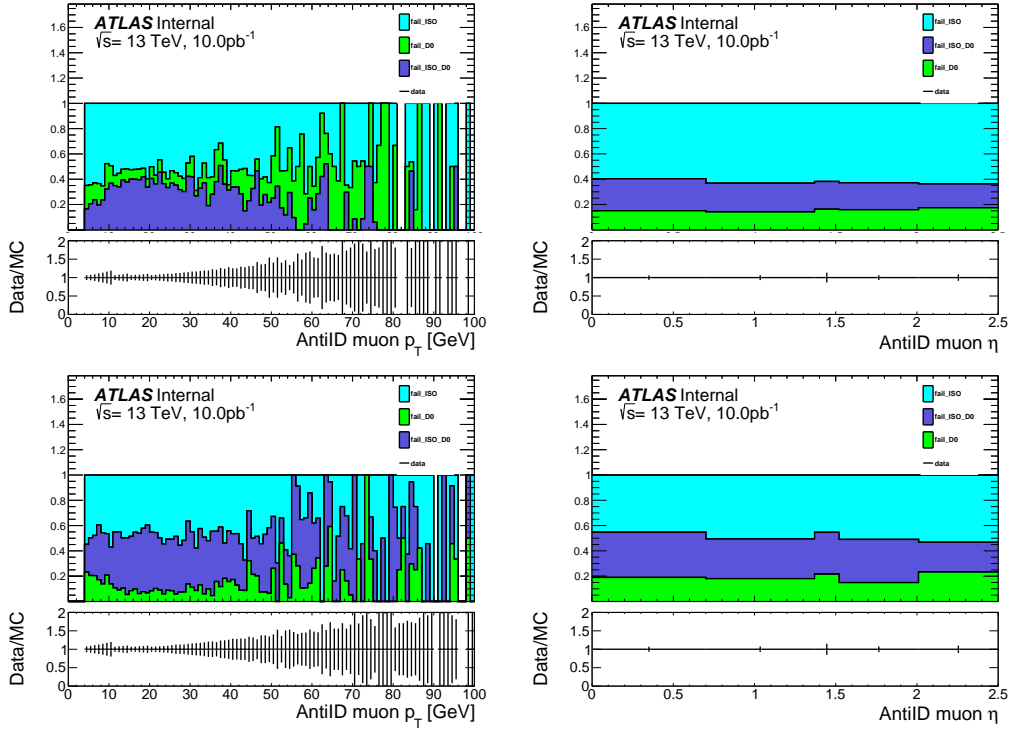


Figure 34: Anti-ID muon composition in events with exactly zero b -jets (top) and one or more b -jets (bottom) as a function of denominator muon p_T (left) and as a function of denominator muon η (right) for events with $m_T < 40$ GeV.

where the fake factor F is computed in discrete p_T bins with different single-muon triggers applied. The specific trigger applied to each range in lepton p_T was chosen to reduce the effect of the trigger turn on and maintain good statistics. Muon p_T distributions for the prescaled triggers shown in Fig. 39 are arbitrarily normalized to 1 pb^{-1} . HLT_mu4 trigger is required for muon p_T $4 - 11$ GeV, HLT_mu10 is required for muon p_T $11 - 15$ GeV, HLT_mu14 is required for muon p_T $15 - 20$ GeV, and HLT_mu18 is required for muon p_T > 20 GeV. A table of these triggers and corresponding p_T range is shown in Table 4

Muon fake factors depend strongly on muon p_T , but also display a systematic dependence on the leading jet p_T . Unlike the electron fake factors, there is also a separate dependence on b -jet multiplicity. Fig. 40 shows the muon fake factors as functions of muon p_T , leading jet p_T , and b -jet multiplicity before any hard jet requirement. Similar to the electron fake factor calculation, the fake factor measurement region requires a hard jet of p_T greater than 100 GeV, but unlike the electron fake factors, the muon fake factors are also separated into two b -jet multiplicity bins: exactly zero b -jets, and one or more b -jets. The bin with exactly zero b -jets is used to estimate the fake contribution in the signal

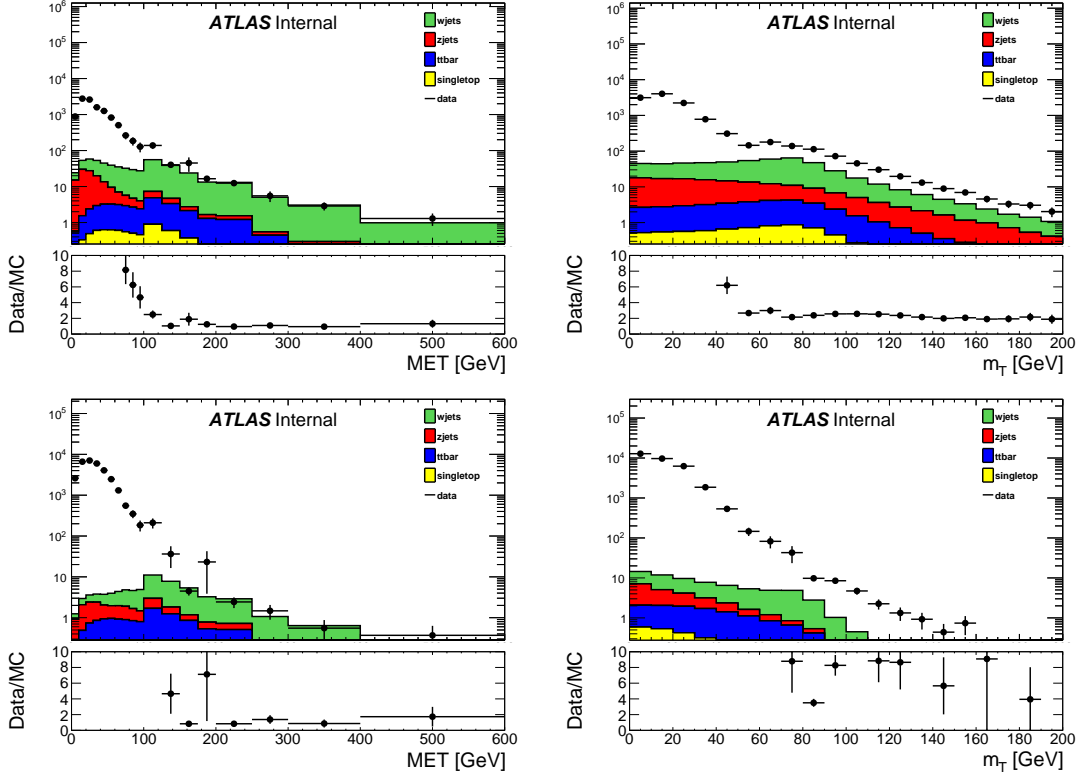


Figure 35: The E_T^{miss} (left) and m_T (right) distributions for numerator (top) and denominator (bottom) muons in the prescaled single-lepton-trigger sample for events with exactly zero b -jets. MC has been scaled to the data in the $E_T^{\text{miss}} > 200$ GeV region.

el trigger	p_T range [GeV]
HLT_mu4	4–11
HLT_mu10	11–15
HLT_mu14	18–20
HLT_mu18	> 20

Table 4: Single-muon triggers used for fake factor computation and their corresponding p_T range.

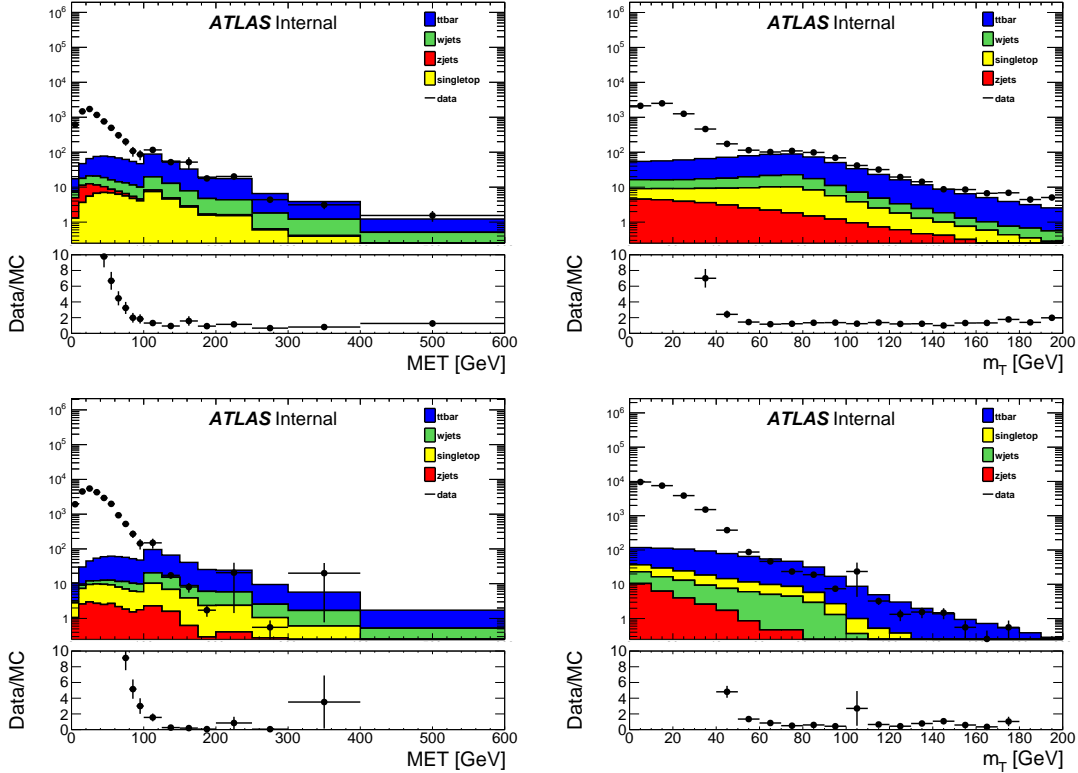


Figure 36: The E_T^{miss} (left) and m_T (right) distributions for numerator (top) and denominator (bottom) muons in the prescaled single-lepton-trigger sample for events with one or more b -jets. MC has been scaled to the data in the $E_T^{\text{miss}} > 200$ GeV region.

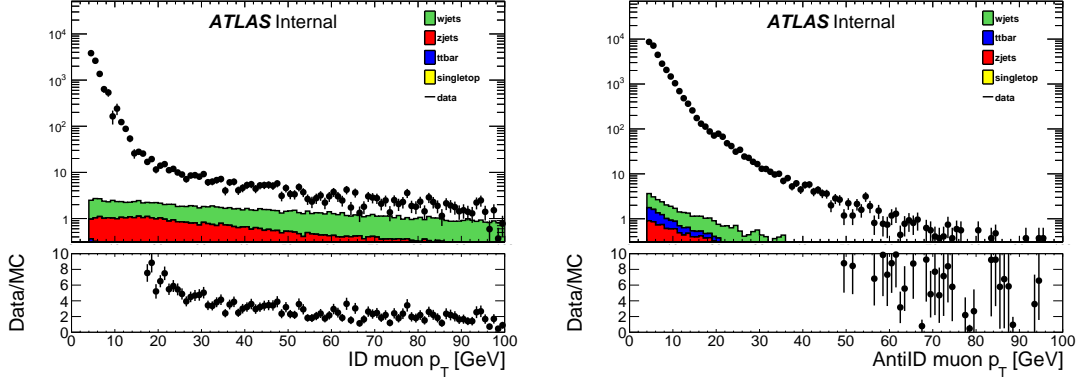


Figure 37: Muon p_T for numerator (left) and denominator (right) objects in the prescaled single-muon trigger sample for events with $m_T < 40$ GeV. MC has been scaled to the data in the $m_T > 100$ GeV region. Distributions from [\[Boerner:2231917\]](#).

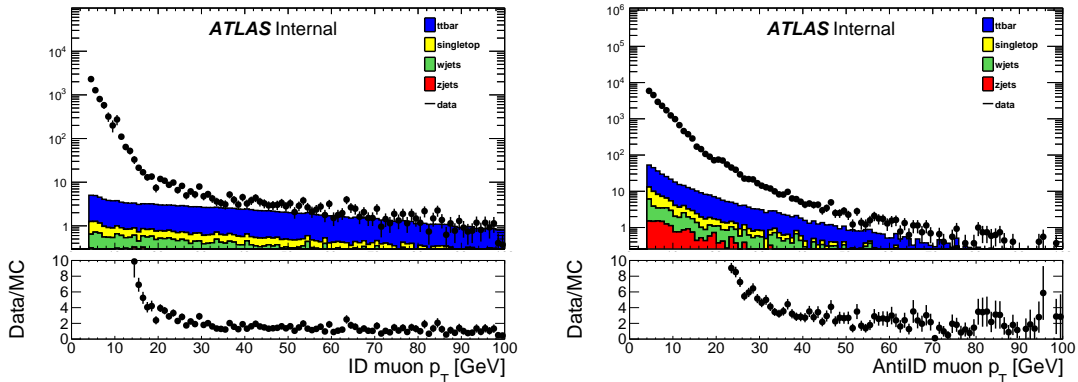


Figure 38: Muon p_T for numerator (left) and denominator (right) objects in the prescaled single-muon trigger sample for events with $m_T < 40$ GeV. MC has been scaled to the data in the $m_T > 100$ GeV region. Distributions from [\[Boerner:2231917\]](#).

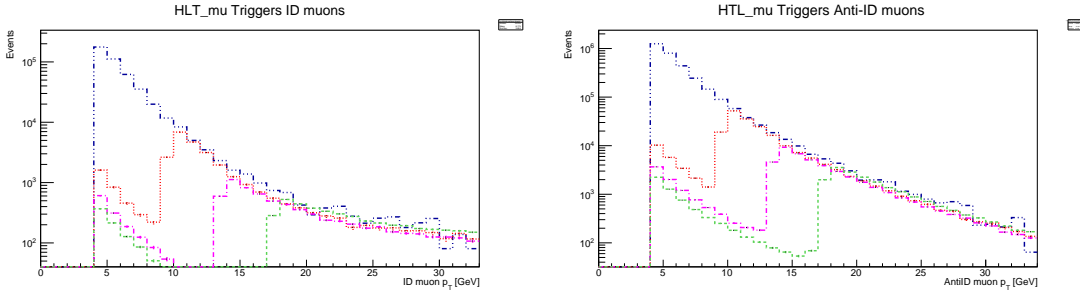


Figure 39: The numerator muon (left) and denominator denominator (right) p_T distributions for prescaled single-muon triggers, normalized to 1 pb^{-1} . Blue curve: HLT_mu4, red curve: HLT_mu10, purple curve: HLT_mu14, green curve: HLT_mu18.

region, and the bin with one or more b -jets is used to estimate the fake contribution in the $t\bar{t}$ control region.

The final fake factors are shown in Fig. 41 as a functions of muon p_T for each of the b -jet multiplicity bins. In addition to the final fake factors binned in p_T , fake factors binned in other variables are also inspected to check for significant trends:

- Fake factors as a function of muon η are shown in Fig. 42,
- Fake factors as a function of $\Delta\phi_{jet1-met}$ are shown in Fig. 43,
- Fake factors as a function of jet multiplicity are shown in Fig. 44,
- Fake factors as a function of average interactions per bunch crossing are shown in Fig. 45,
- Fake factors as a function of the number of primary vertices are shown in Fig. 46.

The relative uncertainties on the muons fake factors versus muon p_T for the separate b -jet multiplicity bins are show in Fig. 47.

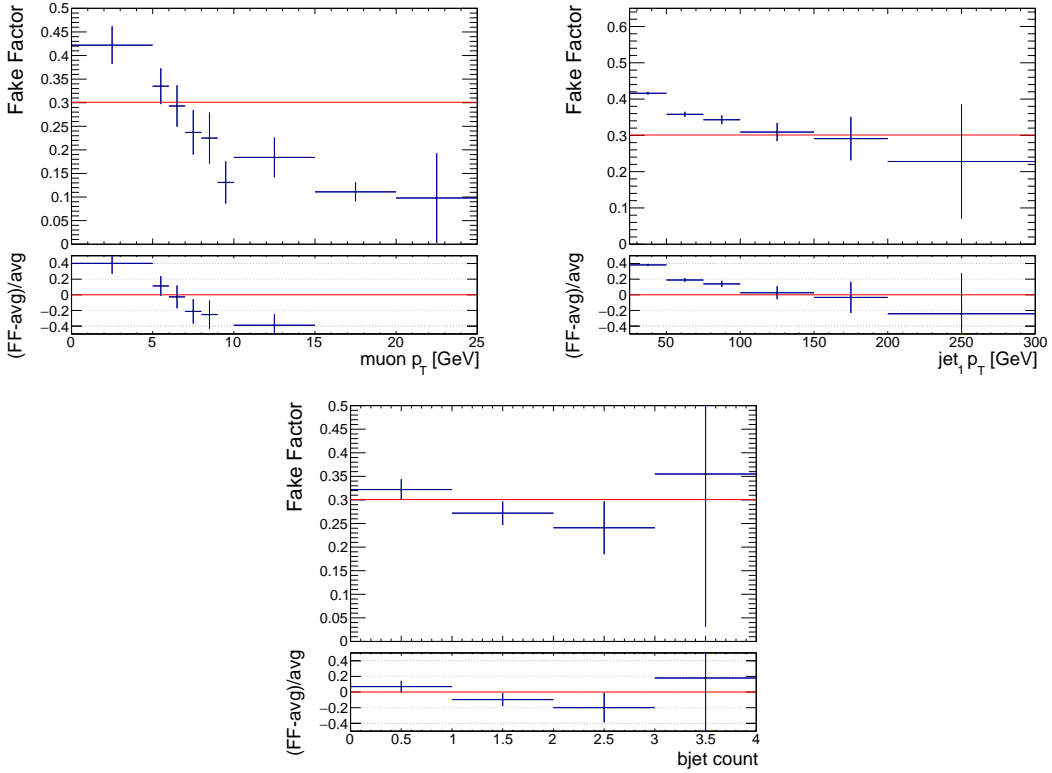


Figure 40: Muon fake factors *before* requiring a hard jet of $p_T > 100 \text{ GeV}$, computed from single-muon prescaled triggers as a function of muon p_T (top-left), as a function of leading jet p_T (top-right), and as a function of b -jet multiplicity (bottom). A red line denotes the average muon fake factor over all muon p_T .

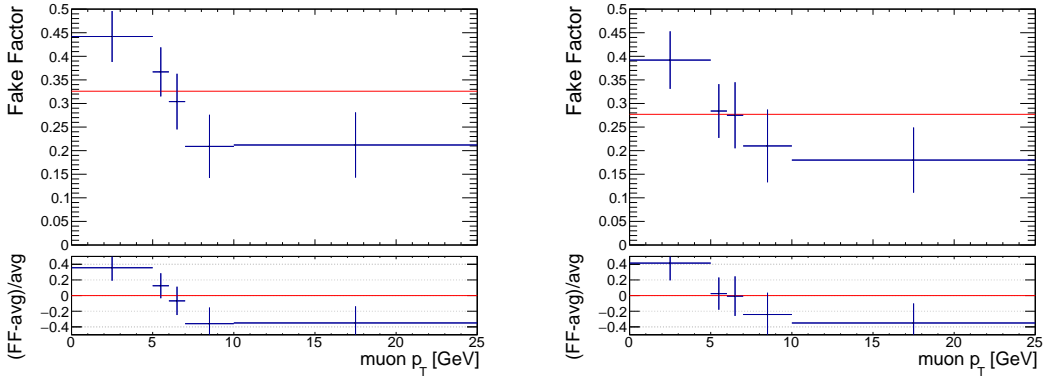


Figure 41: Muon fake factors computed from single-muon prescaled triggers as a function of muon p_T in events with exactly zero b -jets (left) and one or more b -jets (right). A red line denotes the average muon fake factor over all muon p_T .

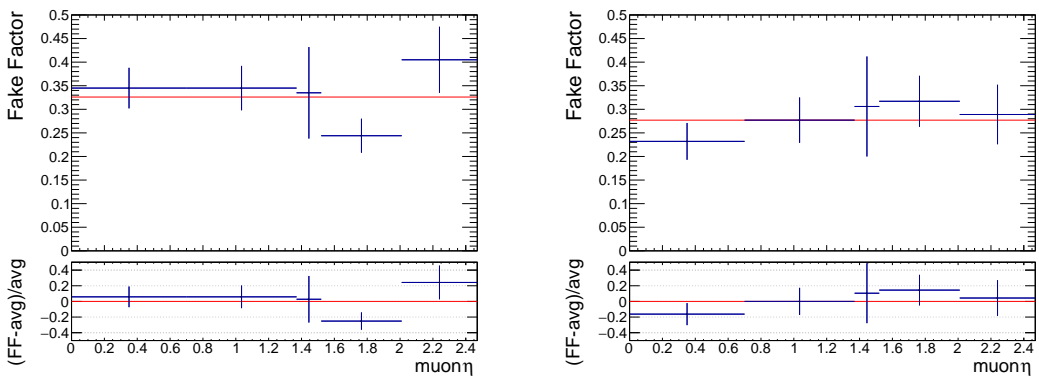


Figure 42: Muon fake factors computed from single-muon prescaled triggers as a function of muon η in events with exactly zero b -jets (left) and one or more b -jets (right). A red line denotes the average muon fake factor over all muon p_T .

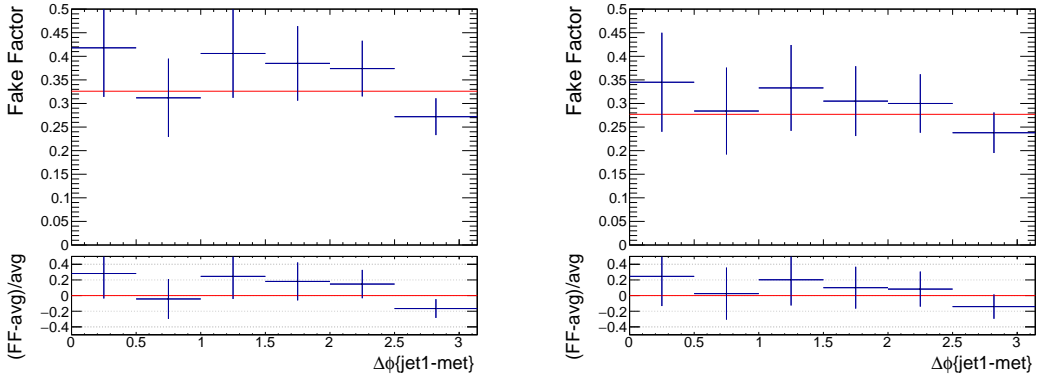


Figure 43: Muon fake factors computed from single-muon prescaled triggers as a function of $\Delta\phi_{\text{jet}-E_{\text{T}}^{\text{miss}}}$ in events with exactly zero b -jets (left) and one or more b -jets (right). A red line denotes the average muon fake factor over all muon p_T

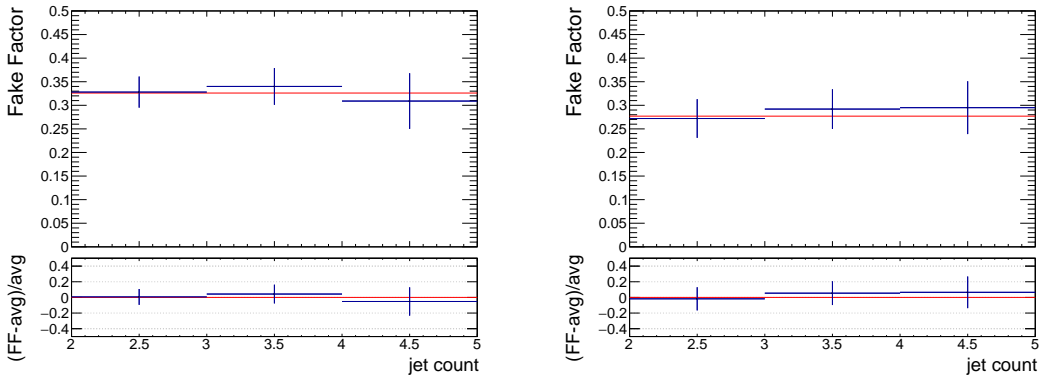


Figure 44: Muon fake factors computed from single-muon prescaled triggers as a function of the jet multiplicity in events with exactly zero b -jets (left) and one or more b -jets (right). A red line denotes the average muon fake factor over all muon p_T

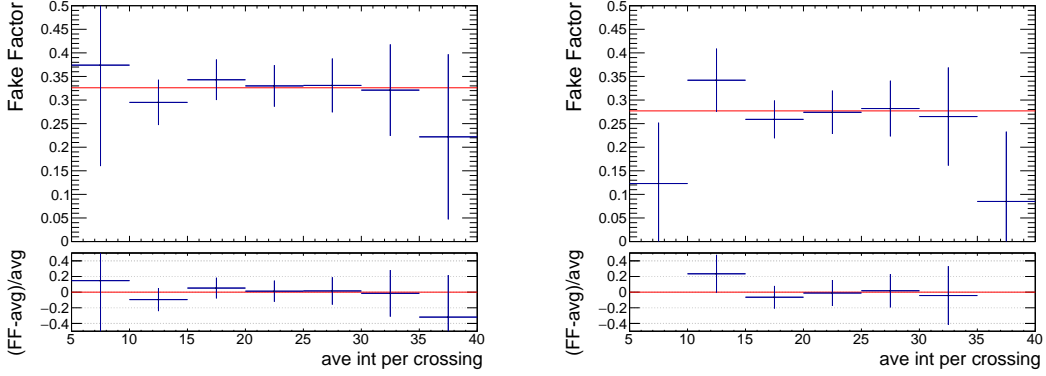


Figure 45: Muon fake factors computed from single-muon prescaled triggers as a function of the average number of interactions per bunch crossing in events with exactly zero b -jets (left) and one or more b -jets (right). A red line denotes the average muon fake factor over all muon p_T

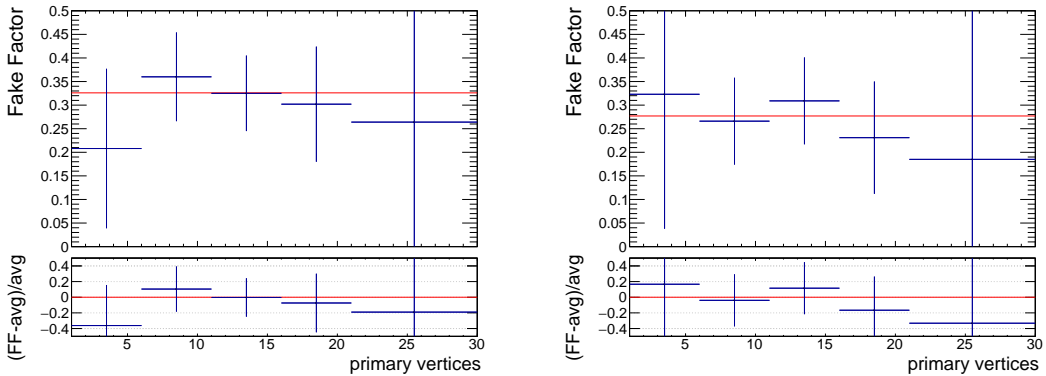


Figure 46: Muon fake factors computed from single-muon prescaled triggers as a function of the number of primary vertices in events with exactly zero b -jets (left) and one or more b -jets (right). A red line denotes the average muon fake factor over all muon p_T

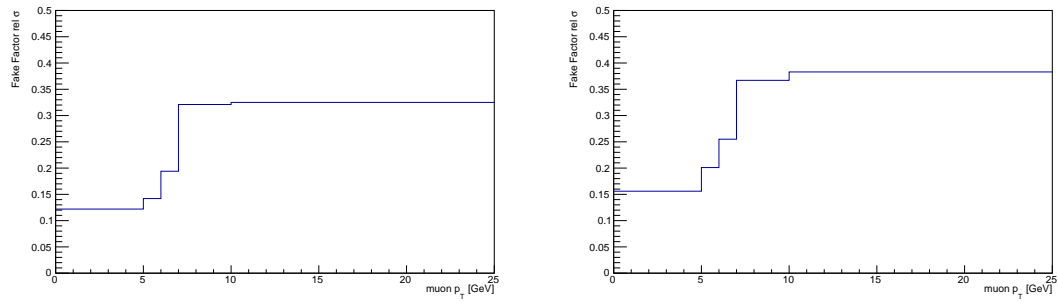


Figure 47: Relative uncertainties on muon fake factors versus muon p_T in zero b -jets bin (left) and one or more b -jets bin (right).

7 Backgrounds

7.1 Fake Lepton Background

Show the calculations and results of the fake estimate. The method will be explained in a dedicated chapter/section.

7.2 $t\bar{t}$ Background

Mainly b-jet requirement

7.3 Drell-Yan Background

Off-shell $z \rightarrow ll$ events.

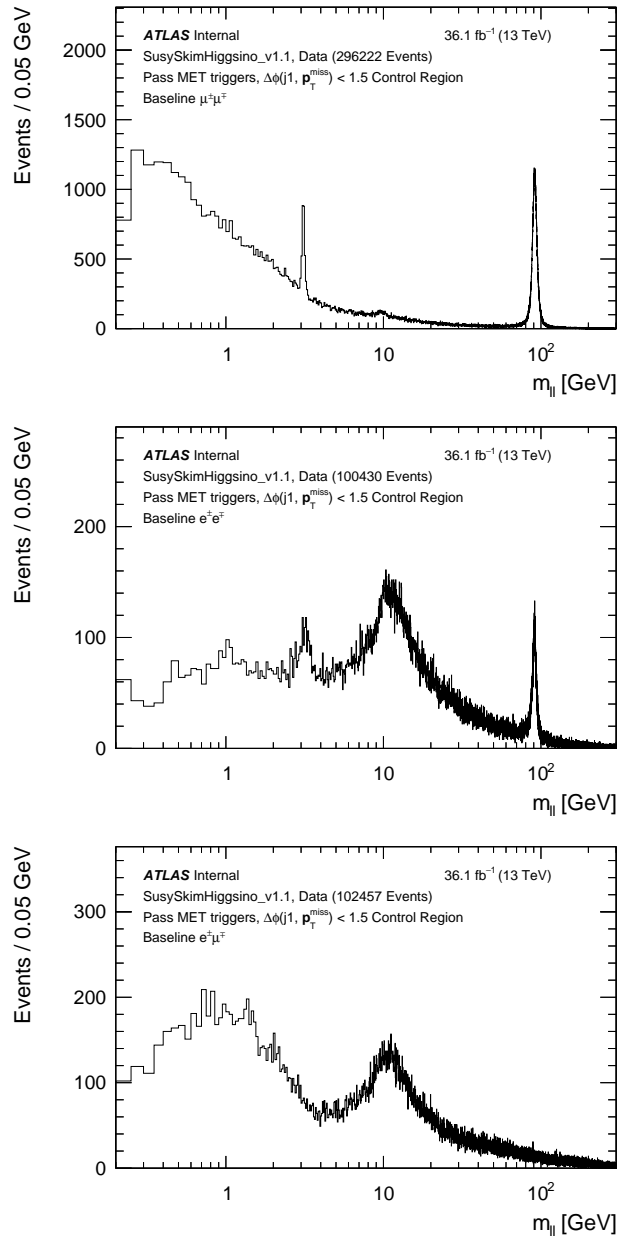


Figure 48: Data events passing inclusive E_T^{miss} triggers with opposite sign baseline leptons in the dilepton invariant mass m_{ll} spectrum. The $\Delta\phi(j_1, \mathbf{p}_T^{\text{miss}})$ variable is inverted to ensure this is orthogonal to the signal region.

7.4 Z+jets Background

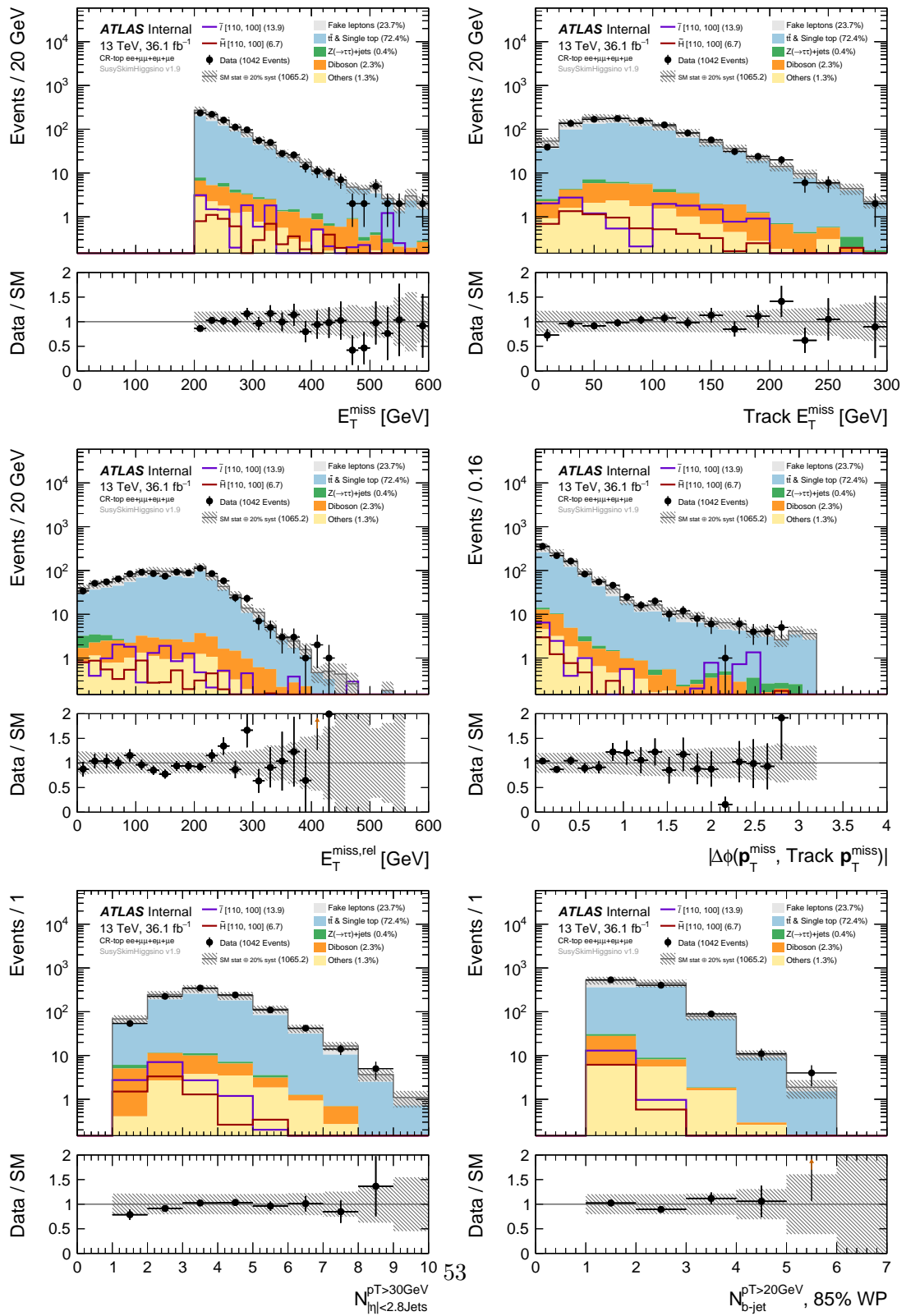


Figure 49: CR-top $ee + \mu\mu + e\mu + \mu e$ channel, pre-fit distributions.

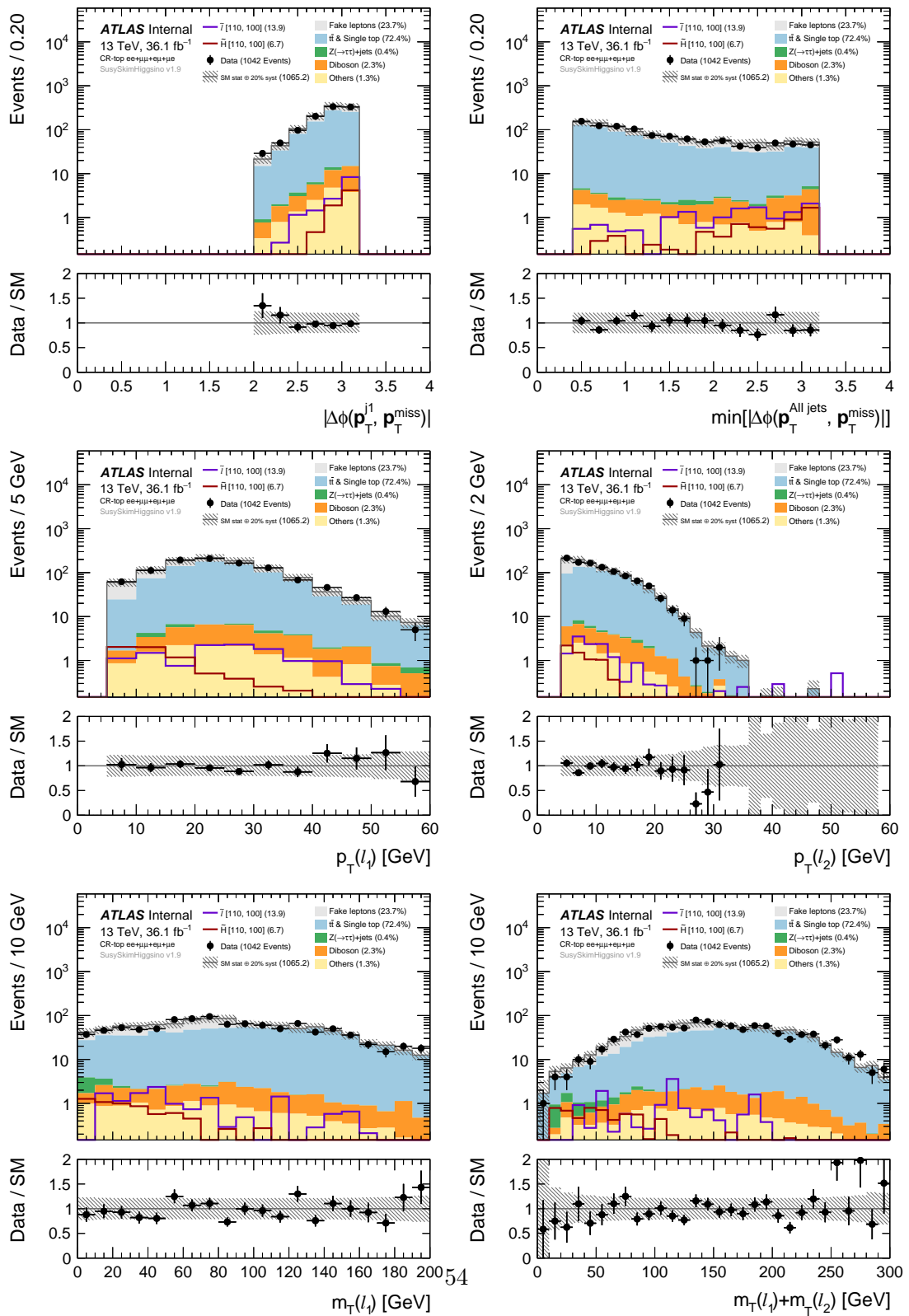


Figure 50: $m_T^{l_1} + m_T^{l_2}$

Figure 51: CR-top $ee + \mu\mu + e\mu + \mu e$ channel, pre-fit distributions.

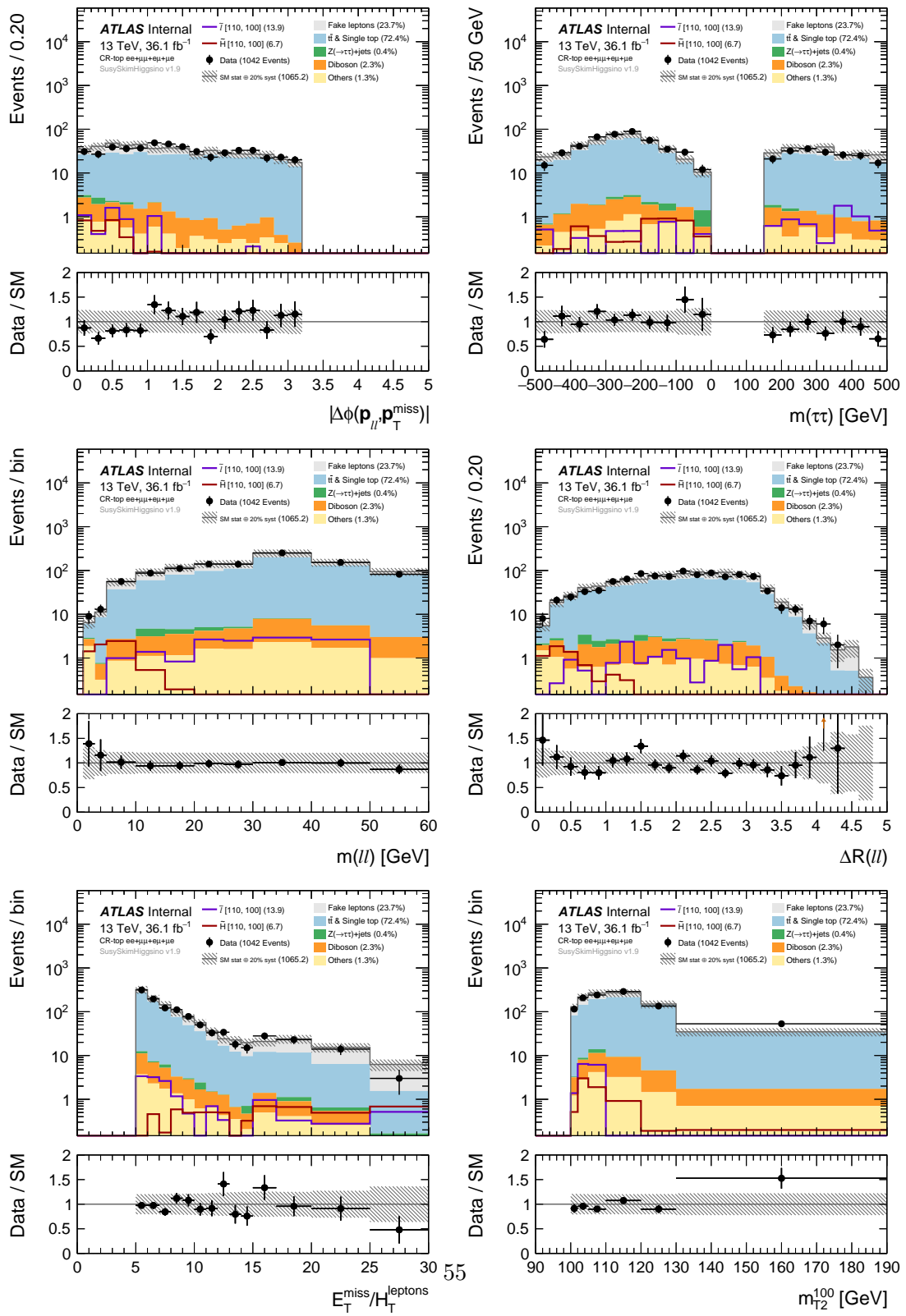


Figure 52: m_{T2}^{100}

Figure 53: CR-top $ee + \mu\mu + e\mu + \mu e$ channel, pre-fit distributions.

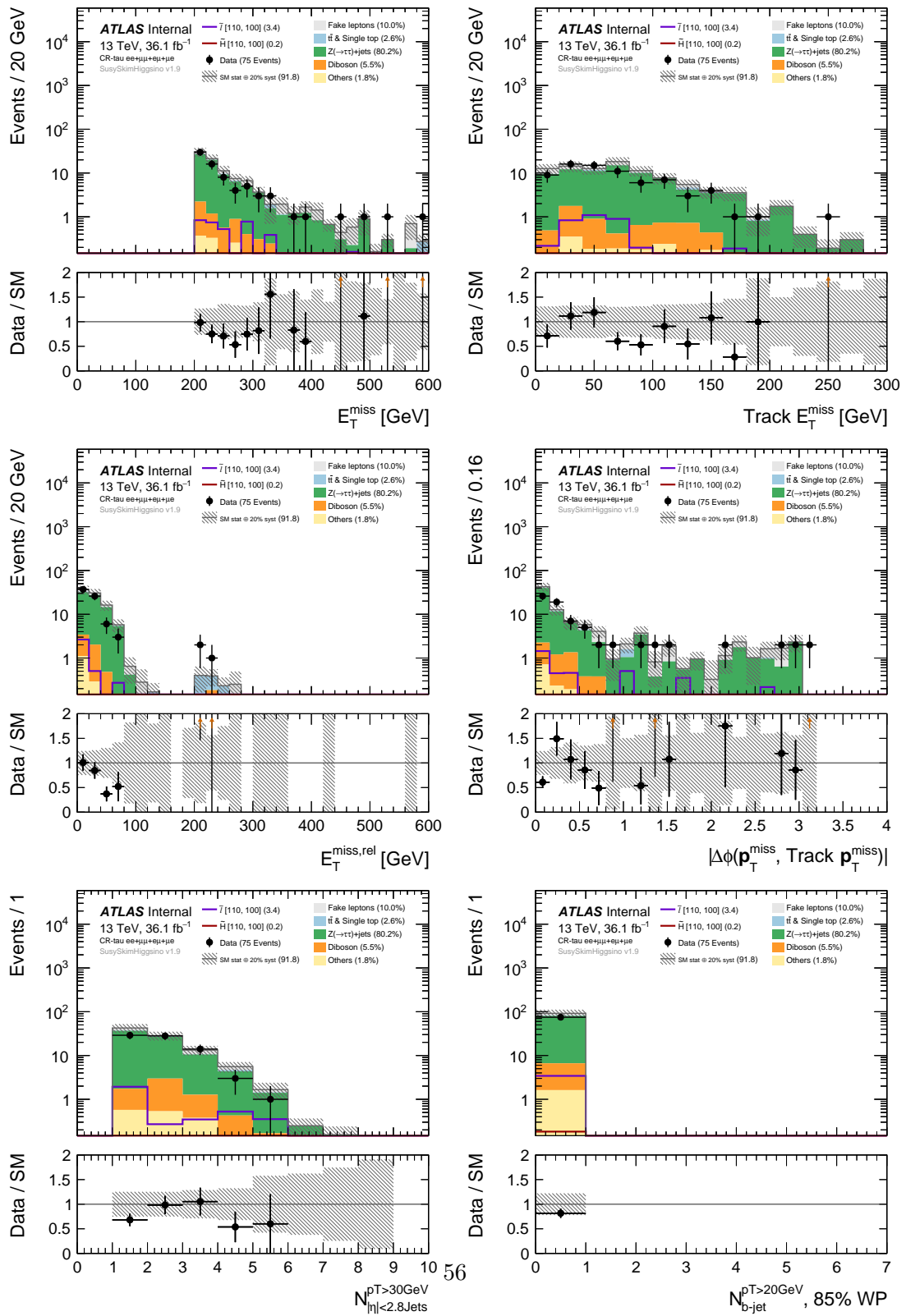


Figure 54: CR-tau $ee + \mu\mu + e\mu + \mu e$ channel, pre-fit distributions.

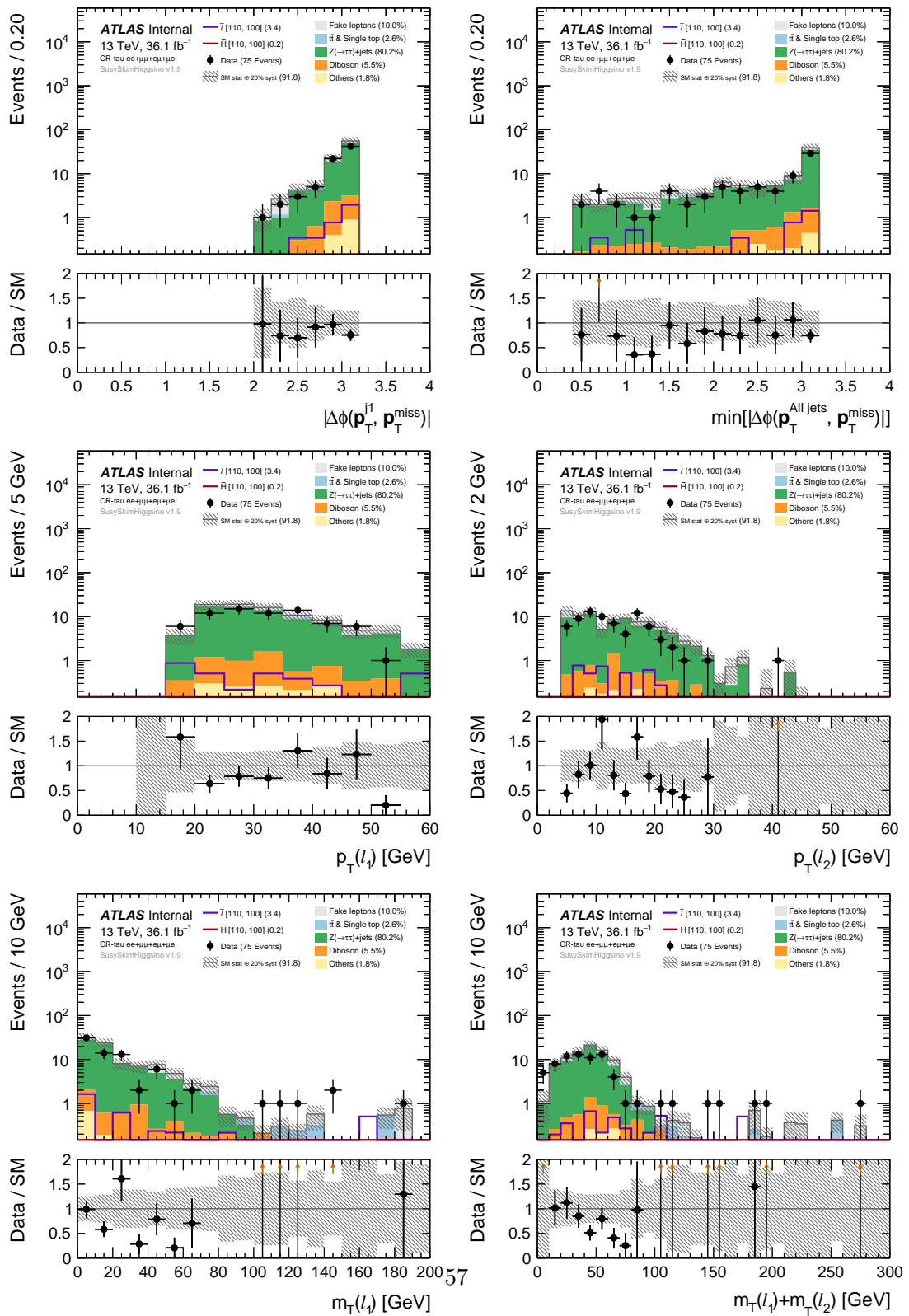


Figure 55: CR-tau $ee + \mu\mu + e\mu + \mu e$ channel, pre-fit distributions.

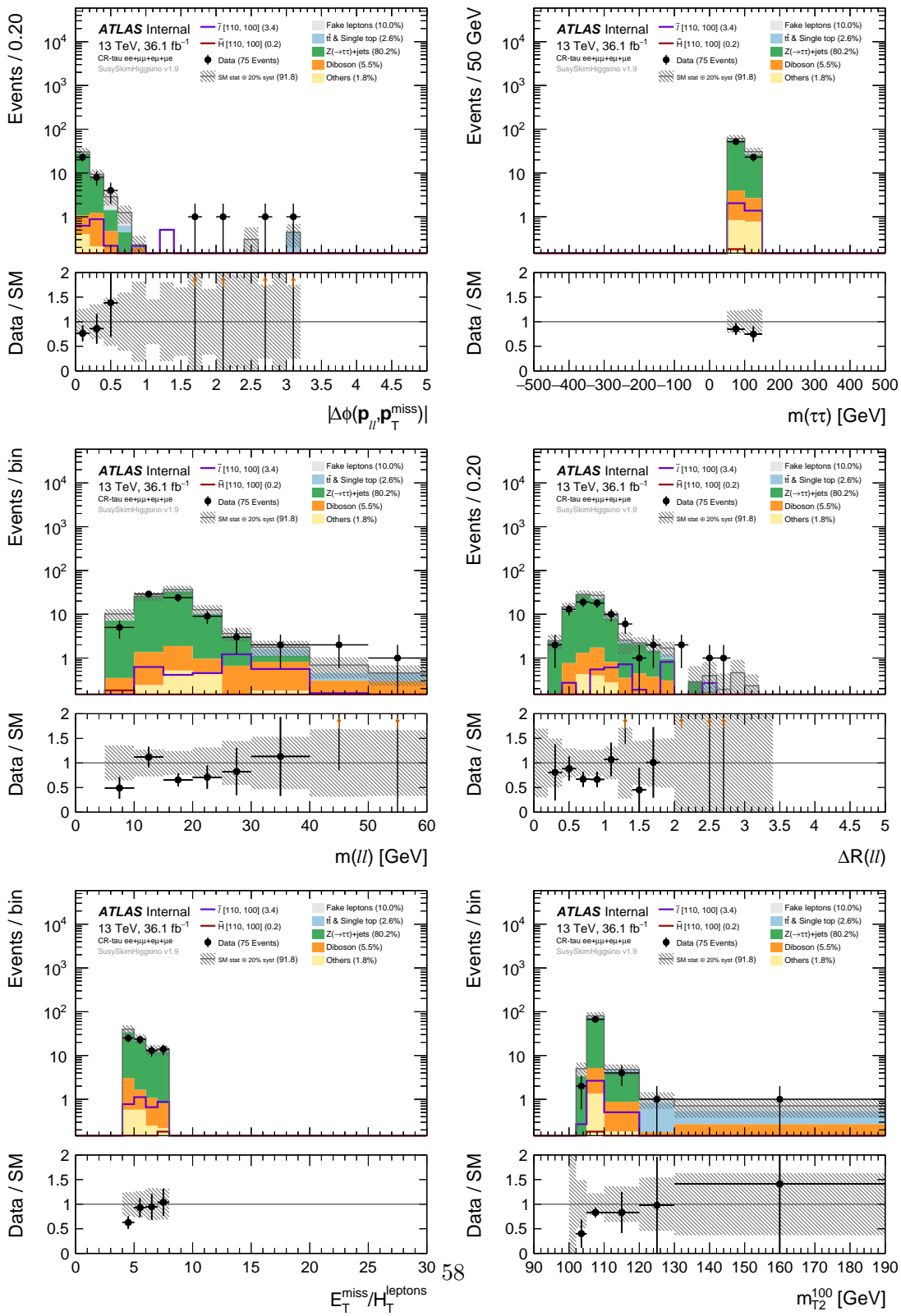


Figure 56: CR-tau $ee + \mu\mu + e\mu + \mu e$ channel, pre-fit distributions.

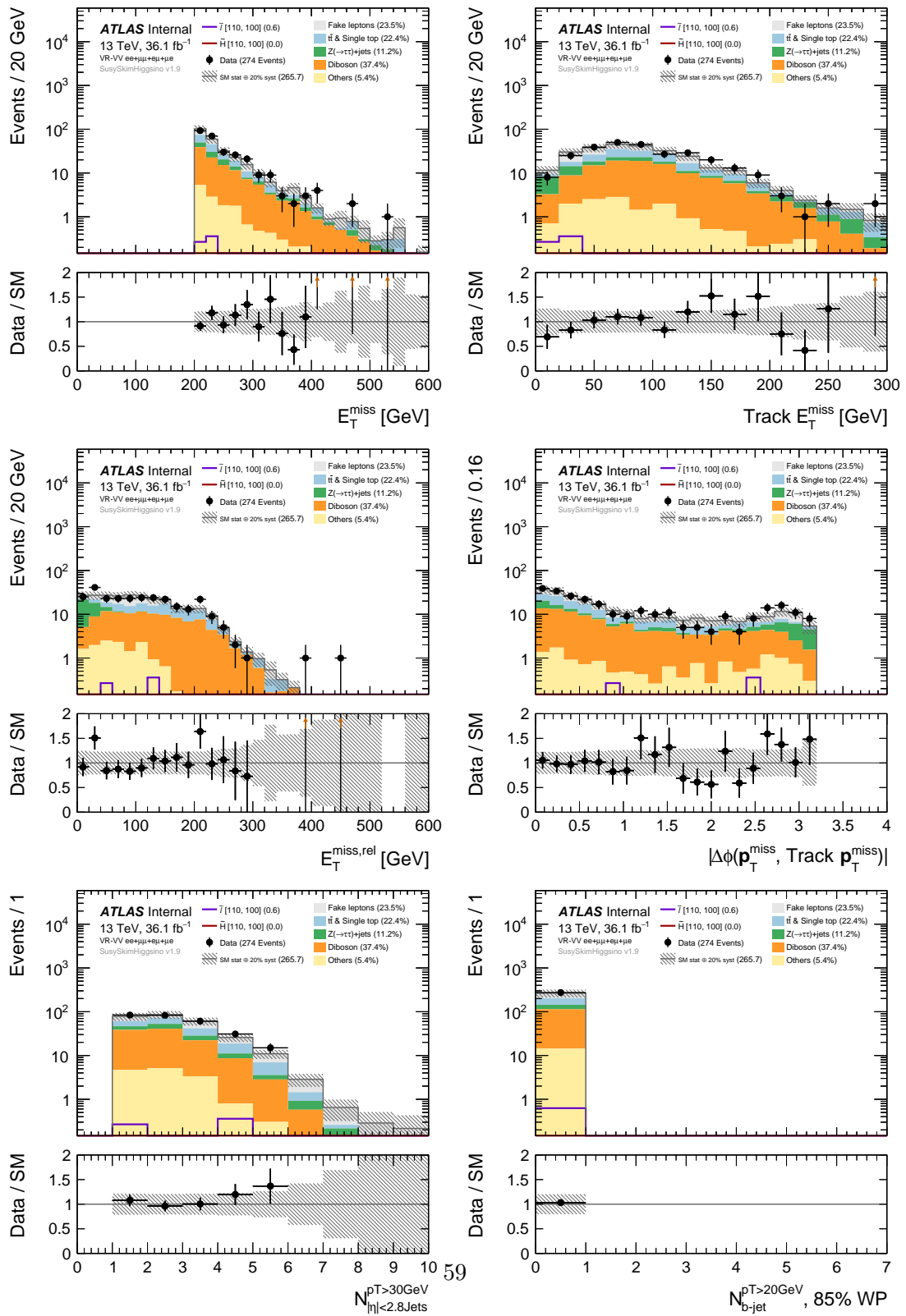


Figure 57: VR-VV $ee + \mu\mu + e\mu + \mu e$ channel, pre-fit distributions.

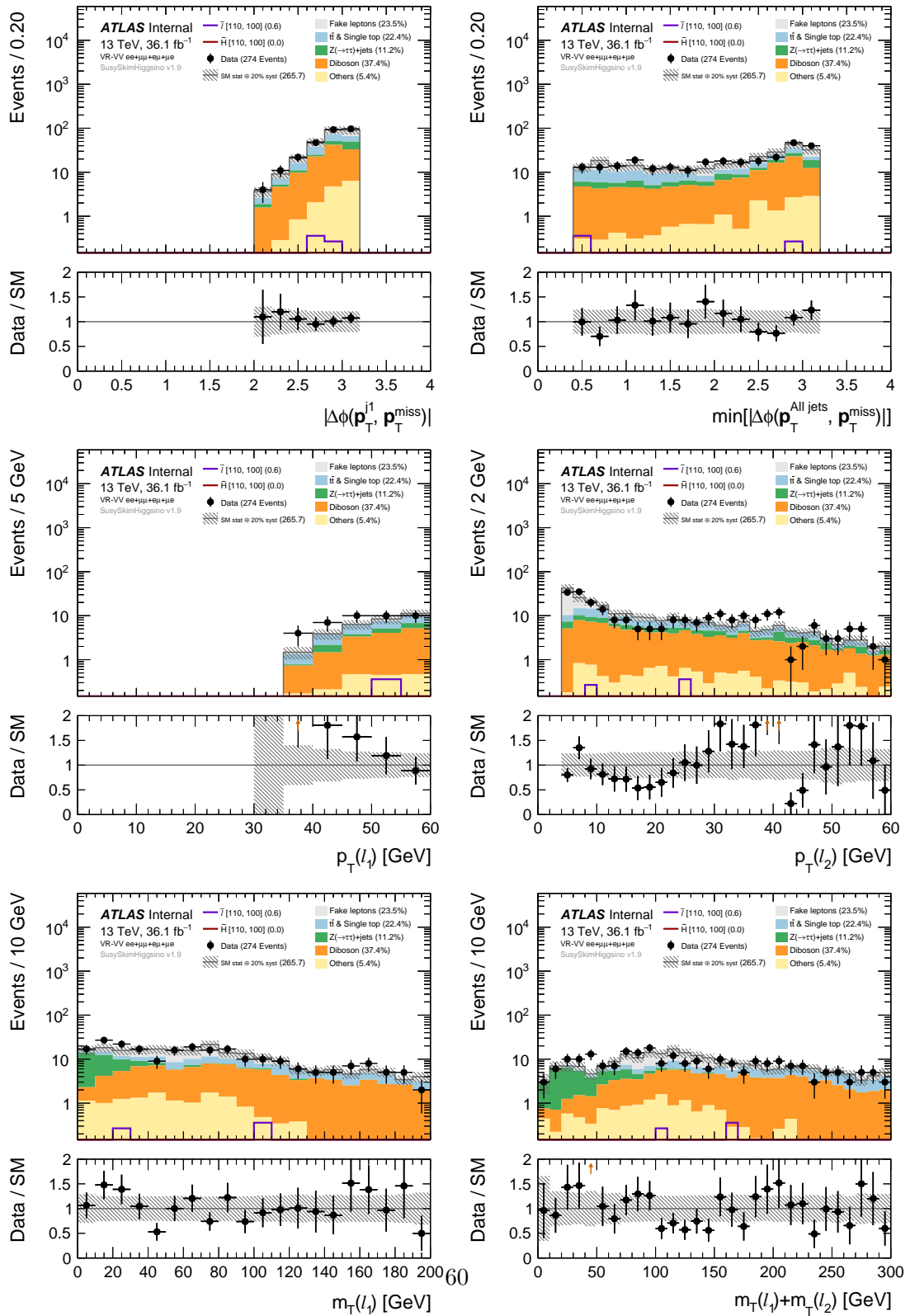


Figure 58: VR-VV $ee + \mu\mu + e\mu + \mu e$ channel, pre-fit distributions.

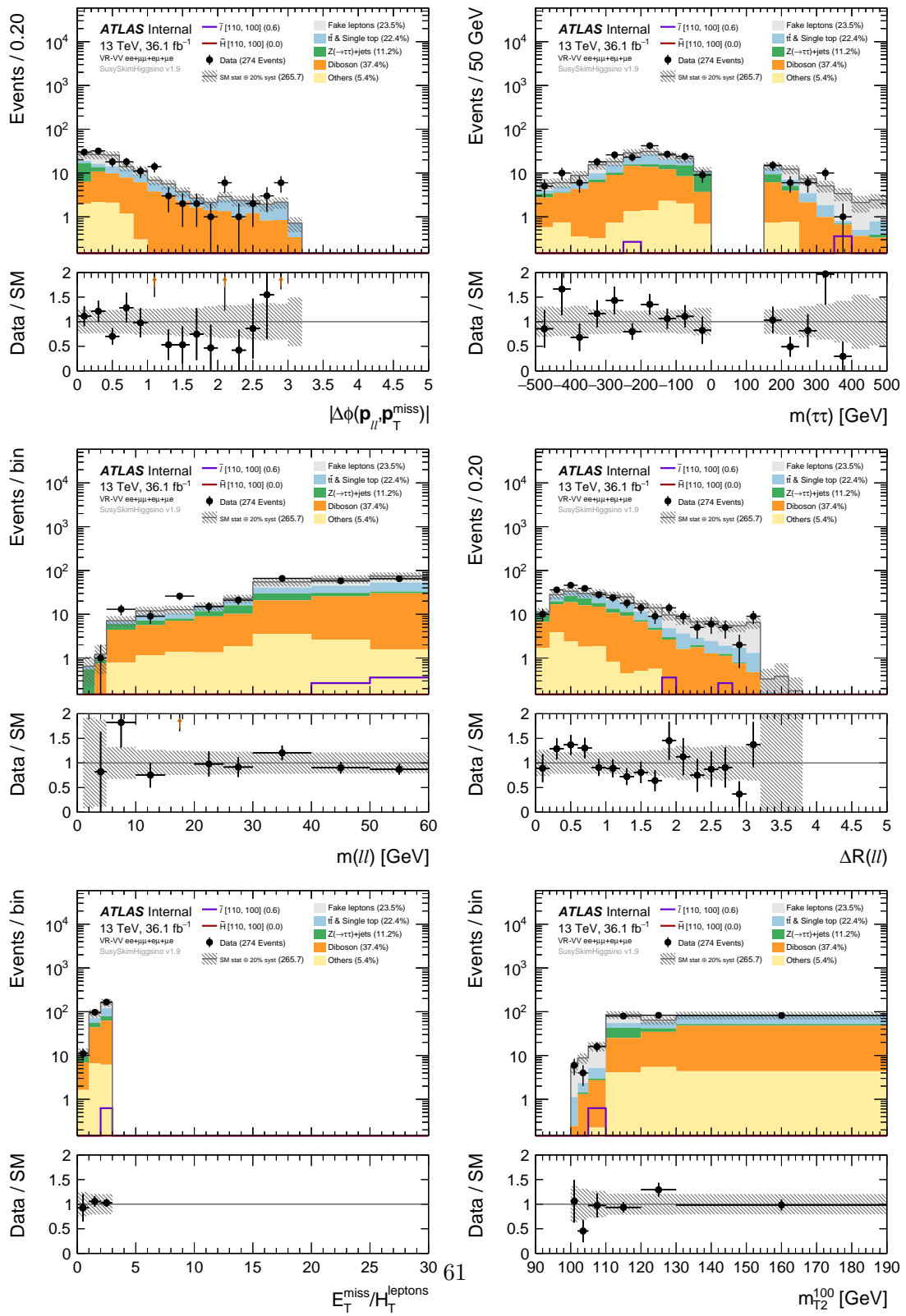


Figure 59: VR-VV $ee + \mu\mu + e\mu + \mu e$ channel, pre-fit distributions.

8 Systematic Uncertainties

Talk about the sources of uncertainty and the estimates.

8.1 Experimental

CP group uncertainties and fake factor uncertainties are the sources of experimental systematics

8.2 Theoretical

In this section we will go over the theoretical systematics and both signal and background estimates.

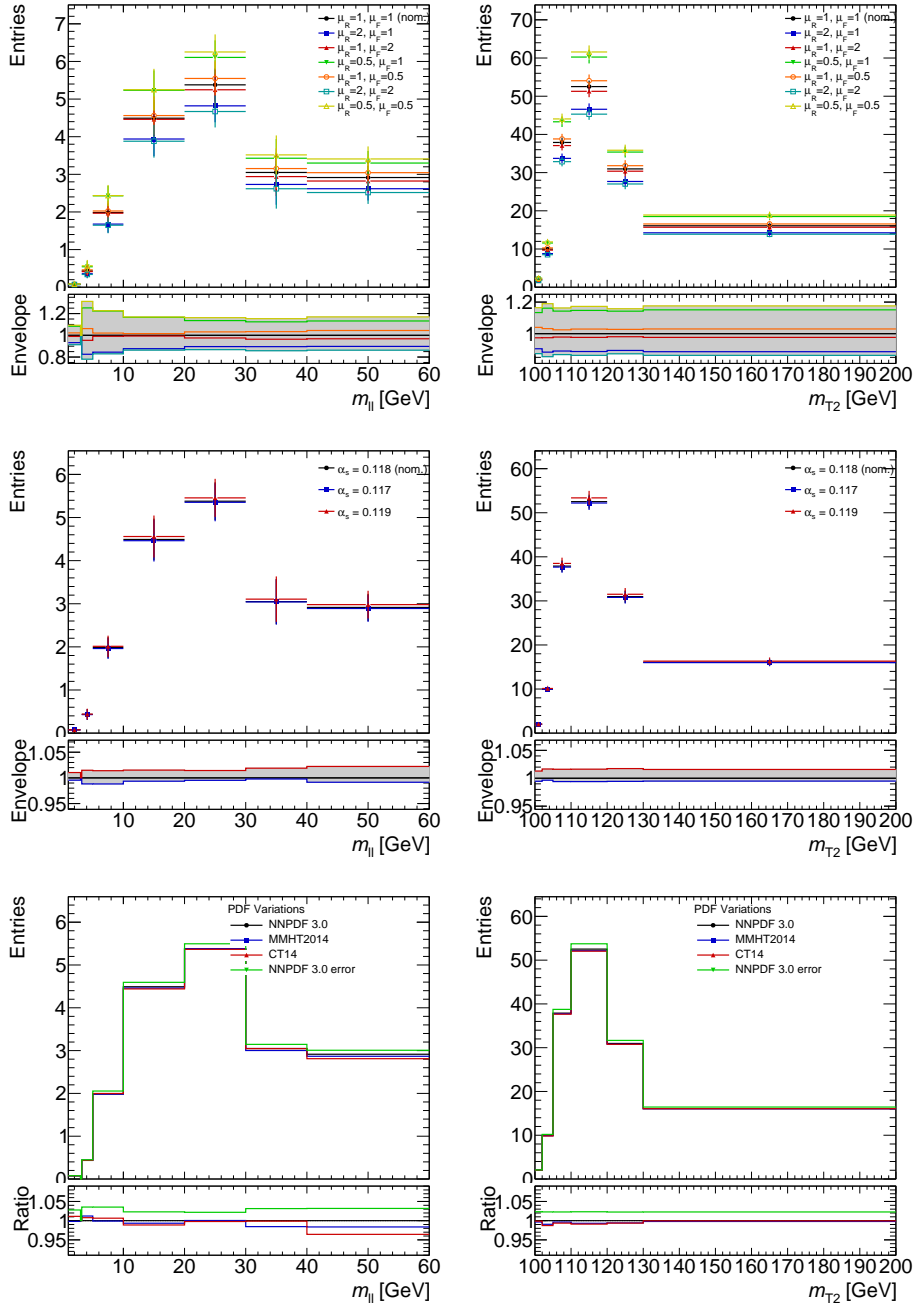


Figure 60: QCD scale, α_s and PDF uncertainties on the shape and normalization of the diboson background in the Higgsino and slepton signal regions (with no lepton flavor requirement).

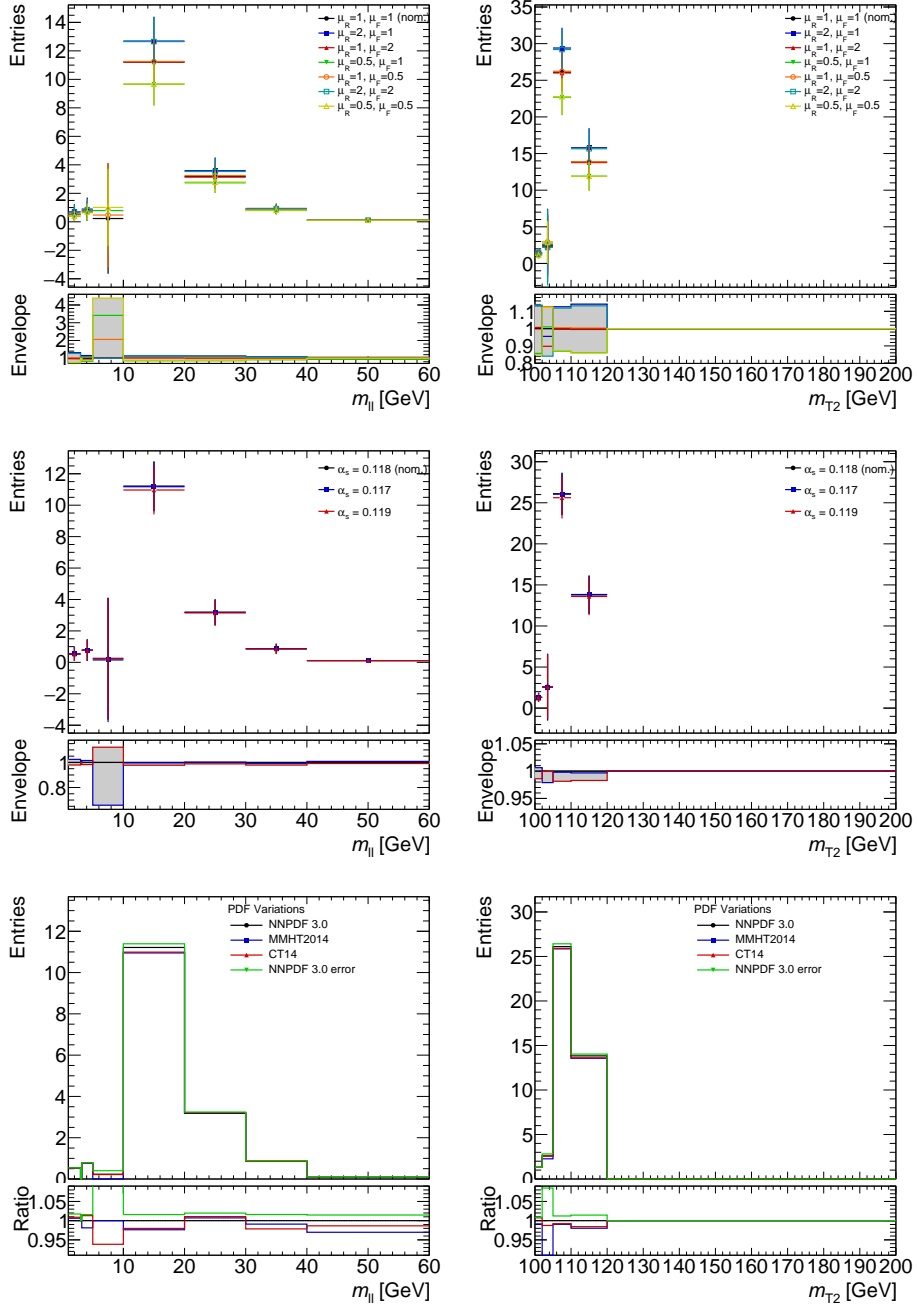


Figure 61: QCD scale, α_s and PDF uncertainties on the shape and normalization of the $Z \rightarrow \tau\tau$ background in the Higgsino and slepton signal regions (with no lepton flavor requirement).

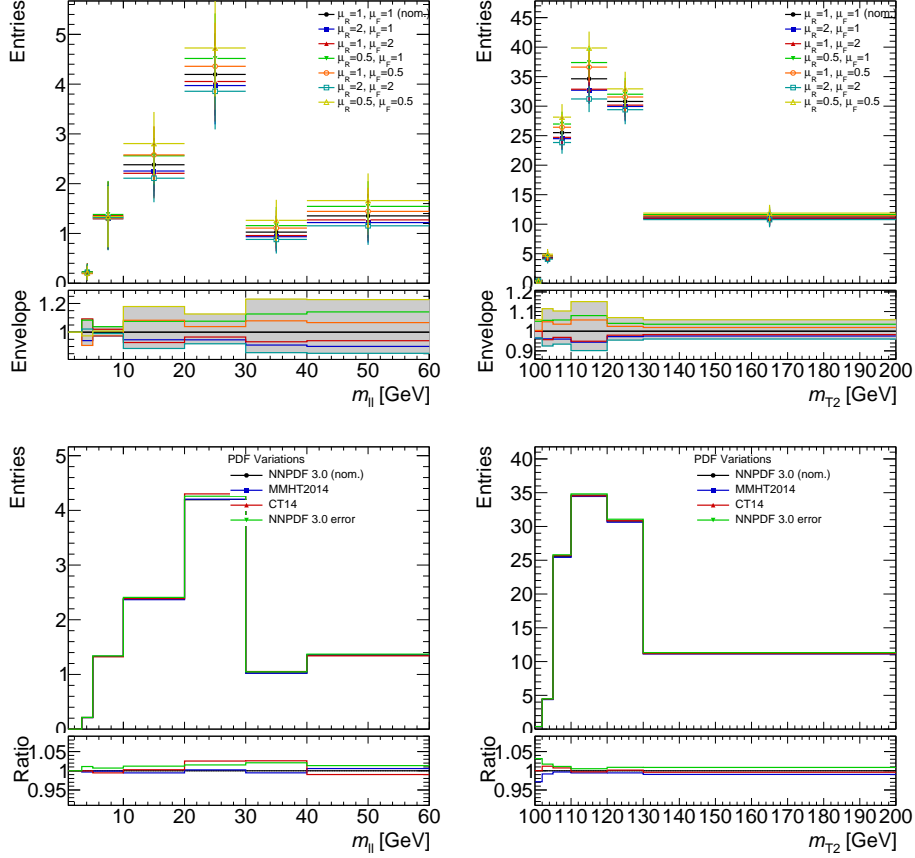


Figure 62: QCD scale and PDF uncertainties on the shape and normalization of the $t\bar{t}$ background in the Higgsino and slepton signal regions (with no lepton flavour requirement).

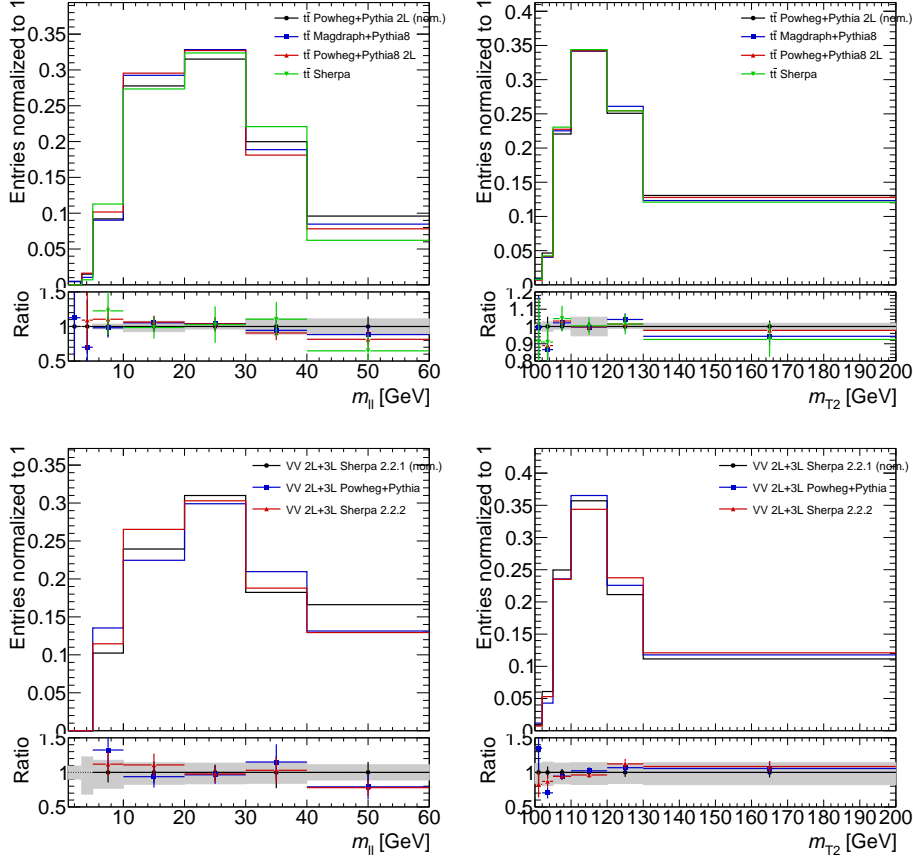


Figure 63: Comparison of the m_{ll} (left) and m_{T2} (right) shapes predicted by different $t\bar{t}$ (top) and VV (bottom) MC generators, in the Higgsino and slepton signal regions. All distributions are normalized to the same number of entries. The gray band displayed in the ratio pad under each distribution represents the modeling uncertainty assigned to each background in each of the bins.

9 Results

Model independent interpretations are shown as well as compressed higgsino and compressed slepton interpretations.

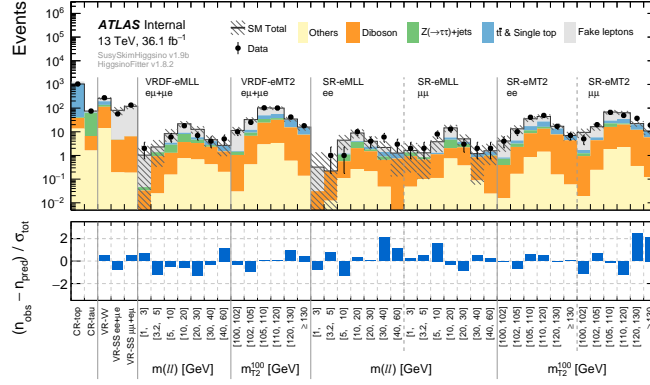


Figure 64: Summary of Monte Carlo yields in control, validation and signal regions in a background-only fit using data only in the two CRs to constrain the fit.

9.1 Compressed Higgsino

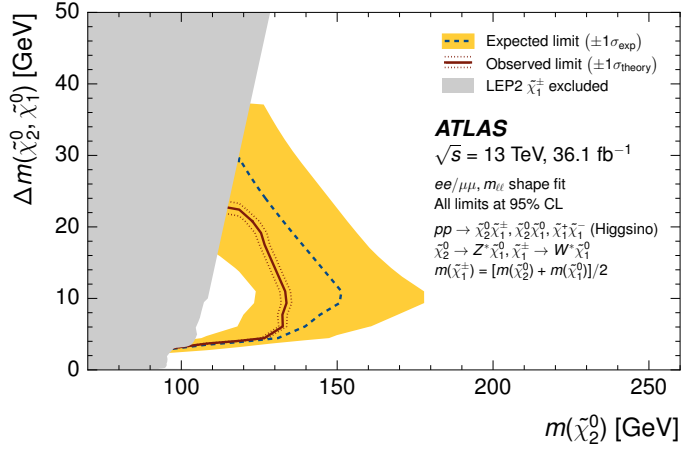


Figure 65: Expected 95% CL exclusion sensitivity (blue dashed line) with $\pm 1\sigma_{\text{exp}}$ (yellow band) from experimental systematics and observed limits (red solid) with $\pm 1\sigma_{\text{theory}}$ (dotted red) from signal cross section uncertainties. A shape fit of Higgsino signals to the $m_{\ell\ell}$ spectrum is used to derive the limit is displayed in the $m(\tilde{\chi}_2^0) - m(\tilde{\chi}_1^0)$ vs $m(\tilde{\chi}_2^0)$ plane. The chargino $\tilde{\chi}_1^\pm$ mass is assumed to be half way between the two lightest neutralinos. The grey region denotes the lower chargino mass limit from LEP [LEPlimits].

9.2 Compressed Slepton

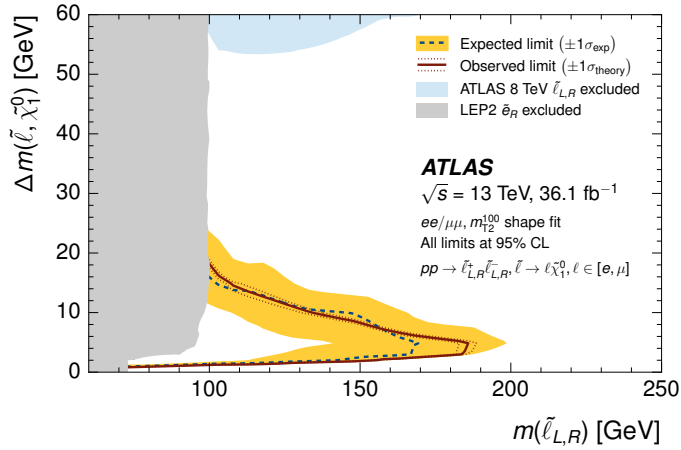


Figure 66: Expected 95% CL exclusion sensitivity (blue dashed line) with $\pm 1\sigma_{\text{exp}}$ (yellow band) from experimental systematics and observed limits (red solid) with $\pm 1\sigma_{\text{theory}}$ (dotted red) from signal cross section uncertainties. A shape fit of slepton signals to the $m_{\tilde{\tau}_2}^{100}$ spectrum is used to derive the limit projected into the $m(\tilde{\ell}) - m(\tilde{\chi}_1^0)$ vs $m(\tilde{\ell})$ plane. The slepton $\tilde{\ell}$ refers to a 4-fold mass degenerate system of left- and right-handed selectron and smuon. The grey region denotes a conservative right-handed smuon $\tilde{\mu}_R$ mass limit from LEP [**LEPlimits**], while the blue region is the 4-fold mass degenerate slepton limit from ATLAS Run 1 [**SUSY-2013-11**].

10 Conclusion

A search for supersymmetry in scenarios with compressed mass spectra was performed using ATLAS data collected in 2015 and 2016 at \sqrt{s} 13 TeV, corresponding to 36.1fb^{-1} . What cool limits we get to put on things because of what we did not see at with LHC data taken by ATLAS detector

References

- [Tul11] Christopher G. Tully. *Elementary Particle Physics in a Nutshell*. Not sure. Princeton University Press, 2011. ISBN: 9780691131160.